

## ABSTRACT

### An Explicit Electron-Vibron Model for Olfactory Inelastic Electron Transfer Spectroscopy

Nishattasnim Liza, M.S.E.C.E.

Mentor: Enrique P. Blair, Ph.D.

The vibrational theory of olfaction was posited to explain subtle effects in the sense of smell inexplicable by models in which molecular structure alone determines an odorant's smell. Amazingly, behavioral and neurophysiological evidence suggests that humans and some insects can be trained to distinguish isotopologue molecules related by isotope substitution. How is it possible to smell a neutron? Inelastic electron transfer spectroscopy (IETS) is a proposed mechanism to explain such subtle olfactory effects: the vibrational spectrum of an appropriately-quantized odorant molecule may enhance a transfer rate in a discriminating electron transfer (ET) process. In contrast to existing models of olfactory IETS, the model presented here explicitly treats the dynamics of the dominant odorant vibrational mode. Power is dissipated directly from electron to environment and indirectly via damped odorant vibrations. The spectroscopic behavior in ET rate is unmasked if the direct-path dissipation is negligible. This may support olfactory isotopomer discrimination.

An Explicit Electron-Vibron Model for Olfactory Inelastic Electron Transfer  
Spectroscopy

by

Nishattasnim Liza, B.S.E.E.C.E.

A Thesis

Approved by the Department of Electrical and Computer Engineering

---

Kwang Y. Lee, Ph.D., Chairperson

Submitted to the Graduate Faculty of  
Baylor University in Partial Fulfillment of the  
Requirements for the Degree  
of  
Master of Science in Electrical and Computer Engineering

Approved by the Thesis Committee

---

Enrique P. Blair, Ph.D., Chairperson

---

Linda J. Olafsen, Ph.D.

---

Kevin L. Shuford, Ph.D.

Accepted by the Graduate School  
May 2019

---

J. Larry Lyon, Ph.D., Dean

Copyright © 2019 by Nishattasnim Liza  
All rights reserved

## TABLE OF CONTENTS

LIST OF FIGURES .....	v
LIST OF TABLES .....	x
ACKNOWLEDGMENTS .....	xi
DEDICATION .....	xii
CHAPTER ONE	
Introduction .....	1
CHAPTER TWO	
Background .....	4
<i>Overview of the Olfactory Process</i> .....	4
<i>Cases Inexplicable by Structural Models</i> .....	5
<i>Motivation for the Vibrational Theory of Olfaction</i> .....	8
<i>Existing Semi-classical Models for the Vibrational Theory of Olfaction</i> ...	8
CHAPTER THREE	
Model .....	12
<i>Framework</i> .....	12
<i>Choice of Parameters</i> .....	16
<i>Justification for a Fully-quantum Treatment</i> .....	16
<i>Calculation of Electron Transfer Time, <math>t_{ET}</math></i> .....	17
<i>Calculation of Power Dissipation, <math>\bar{p}_{diss}</math></i> .....	20
CHAPTER FOUR	
Results .....	21
<i>Indirect Coupling Dominates</i> .....	21
<i>Direct (Electron-environment) Coupling Dominates</i> .....	33
<i>Both Direct and Indirect Coupling are Significant</i> .....	35
CHAPTER FIVE	
Conclusion .....	39
APPENDIX A	
Derivation of Power Expressions .....	42
<i>Power Flow in a Closed System</i> .....	42
<i>Power Flow in an Open System</i> .....	44
BIBLIOGRAPHY .....	47

## LIST OF FIGURES

- Figure 1.1. The inelastic electron tunneling spectroscopy (IETS) mechanism is illustrated in the context of human olfaction. A human odorant receptor is known to be a G-protein coupled receptor (GPCR, shown in blue, with an associated G protein). When an odorant molecule docks in the receptor (left figure), an electron transition from D (quantum state  $|D\rangle$  at energy  $E_D$ ) to A (state  $|A\rangle$  at energy  $E_A$ ) requires a change in energy that is facilitated by the excitation of a quantum of molecular vibrational energy. Once complete, the transferred electron may trigger the activation of the associated G protein, leading to an action potential and a sensory detection event. Without an odorant having a properly-quantized vibrational spectrum, the electron transition and subsequent detection are much less probable. .... 3
- Figure 2.1. An overview of the olfactory process in humans. Odorant molecules enter the nasal cavity and approach the olfactory epithelium [frame (a)]. Odorants must diffuse through a mucus layer prior to reaching the olfactory epithelium [frame (b)]. At the epithelium, odorants must interact with olfactory receptors on the olfactory cilia projecting from the olfactory sensory neuron's dendritic process [1]..... 4
- Figure 2.2. (a) Ferrocene,  $\text{Fe}(\text{C}_5\text{H}_5)_2$  and nickelocene,  $\text{Ni}(\text{C}_5\text{H}_5)_2$  have very similar structures but have distinctly different scents. (b) Cis-nor-ketone (4-(4-tert-butylcyclohexyl)-4-methylpentan-2-one) and cis-ketone (4-(4-tert-butylcyclohexyl)-4-methylhexan-2-one) are very similar in structure but the former is said to be nearly odorless and the latter is said to have a "penetrating urine odor". .... 6
- Figure 2.3. Commonly-occurring acetophenone (ACP-h) (left) and its fully-deuterated isotomer acetophenone-d8 (ACP-d)(right). They are structurally and electronically very similar. .... 7

Figure 3.1. The model developed in this paper includes the explicit, fully-quantum treatment of a  $|D\rangle \rightarrow |A\rangle$  electron transfer event (ET) coupled to a dominant odorant vibrational mode. The “Electronic state” represents the ET event, and the “Vibrational system” represents the dominant odorant mode. This ET event is coupled to the thermal environment both directly, and indirectly via the odorant vibrational mode. In each case, the parameter that characterizes coupling between two systems is listed. 13

Figure 3.2. A fully-quantum treatment within the vibrational theory of olfaction is justified. The eigenvalues of the fully-quantum Hamiltonian  $\hat{H}$  are plotted relative to the Marcus-type potential energy surfaces  $V_k^{(M)}(Q)$  vs.  $Q$ . This plot is shown for two different values of the odorant reorganization energy  $\lambda$ : once with  $\lambda = 30$  meV and again with  $\lambda = 300$  meV. In each case, the energy discretization of fully-quantum system is significant compared to feature sizes of semi-classical adiabatic Marcus-type potential surfaces. This suggests that treatment using the fully-quantum model will lead to behaviors not captured by a Marcus-type semi-classical model. .... 18

Figure 3.3. Calculation of threshold defined electron transition time,  $t_{ET}$ , from the dynamic solution to Eqn. (3.5). Here,  $\hat{\rho}(t)$  is calculated and the probabilities  $P_D$  and  $P_A$  for finding the electron on  $D$  or  $A$  are calculated.  $t_{ET}$  is defined as the time when  $P_D$  drops from  $P_D(0) \simeq 1$  to a threshold value  $P_D^{(thresh)}$ . When  $P_D^{(thresh)} = 0.2$ , the result is  $t_{ET} = 37.5$  ps. Dashed black lines indicate the threshold  $P_D^{(thresh)} = 0.2$  and the electron-transfer time,  $t = t_{ET}$ , defined as the time that  $P_D$  drops below  $P_D^{(thresh)}$ . .... 19

Figure 4.1. The electron transfer rate,  $k$ , from state  $|D\rangle$  to state  $|A\rangle$  exhibits resonant tunneling and environmentally-driven broadening of peaks. Here, peaks occur under a resonant condition that arises when the detuning  $\Delta = E_D - E_A$  is equal to an integer multiple of the vibrational quantization  $\hbar\omega_o$ . Additionally, resonant peaks are broadened as odorant-environment coupling increases, as quantified by  $\chi_v$ . .... 22

- Figure 4.2. The eigenenergy spectrum for the system results in a resonant effect for the ET rate  $k$ . In the limit of  $\gamma = \lambda = T = 0$ , the eigenstates are  $|Xn\rangle$ , with energies  $E_X + \hbar\omega (n + 1/2)$ . When  $\Delta = E_D - E_A = s\hbar\omega$  for some integer  $s$ , a resonant transition  $|D0\rangle \rightarrow |As\rangle$  is favorable, as is the resonant back-transition  $|As\rangle \rightarrow |D0\rangle$ . The probability  $P_D$  does not decrease to a small value until the system can dissipate energy for the state to approach  $|A0\rangle$ . Since this dissipation takes time, the minimum non-zero value ( $n = 1$ ) enables the fastest dissipation and thus the fastest ET time and the highest ET rate  $k$ . 23
- Figure 4.3. Resonant peaks in  $k(f_o)$  are broadened as odorant reorganization energy,  $\lambda$ , is increased. Also, increasing  $\lambda$  contributes to a higher ET rate,  $k$ , for lower frequencies. This is seen in subfigure (a) for a weaker odorant-environment coupling,  $\chi_v = 1/2$ , and again in subfigure (b) for a stronger coupling,  $\chi_v = 2$ . . . . . 24
- Figure 4.4. Increase in tunneling energy,  $\gamma$ , contributes to higher electron transfer rate,  $k$ , from state  $|D\rangle$  to state  $|A\rangle$ . This is shown for weak odorant-environment coupling,  $\chi_v = 1/2$  in subfigure (a) and for strong odorant-environment coupling,  $\chi_v = 2$  in subfigure (b). . . . . 25
- Figure 4.5. Electron transfer rate,  $k$ , from state  $|D\rangle$  to state  $|A\rangle$  is largely temperature-independent at terrestrial temperatures and below. ET rate is shown here as a function of environmental temperature  $T$  for different values of odorant-environment coupling  $\chi_v$ . When  $T$  is sufficiently large that  $k_B T \sim \hbar\omega$ , ET rate decreases since thermal environmental fluctuations enable  $|A\rangle \rightarrow |D\rangle$  excitation. . . . . 26
- Figure 4.6. Model ET rates exhibit both quantum and classical/semi-classical behaviors over the spectrum of odorant frequencies  $f_o$ . In the low frequency limit ( $\hbar\omega_o \ll \Delta$ ), increasing temperature increases the rate  $k$  in a behavior consistent with a classical or semi-classical system in which thermal excitation allows the system to surmount a classical barrier. In the high-frequency limit ( $\hbar\omega_o \gg \Delta$ ), ET rate,  $k$ , decreases with a significant increase in temperature. This is consistent with the behavior noted in Section 4. . . . . 27

Figure 4.7.	The model developed here exhibits a differential response to isotopomers. (a) A receptor tuned to the C-H stretch responds to the C-H stretch with a rate $k$ that is more than one order of magnitude higher than the rate due to the presence of a C-D stretch vibrational mode. A receptor tuned to the C-D stretch exhibits a similarly higher ET rate when an odorant with a C-D ligand is present than when an odorant with a C-H ligand is present. (b) Peak broadening occurs with stronger odorant-environmental coupling, and the change in rate between isotopomers is reduced for each receptor. ....	29
Figure 4.8.	Power dissipation $\bar{p}_{\text{diss}}$ to the environment exhibits a frequency-dependence very similar to the the frequency dependence of rate $k$ to odorant frequency (compare with Figure 4.1). Peaks for $\bar{p}_{\text{diss}}$ occur when $\Delta = s\hbar\omega_o$ for some integer $s$ , and resonant peaks broaden with stronger odorant-environment interaction (increasing $\chi_v$ ). ....	30
Figure 4.9.	Power dissipation $\bar{p}_{\text{diss}}$ exhibits a linear correlation with ET rate. This scatter plot of rate data from Figure 4.1 and power dissipation data from Figure 4.8 shows a highly linear relationship between the two sets of data. A fitting line is drawn in purple, and the data lies along this same line for several odorant-environment coupling strengths. ....	31
Figure 4.10.	Average power dissipation to the environment is frequency-selective—and therefore ligand-selective. Power dissipation peaks when a receptor tuned to the C-H (or C-D) stretch couples to a ligand with a frequency $f_o$ matching the frequency of the C-H (or C-D) stretch. This is shown for weak odorant-environment coupling, $\chi_v = 1/2$ in subfigure (a) and for strong odorant-environment coupling, $\chi_v = 2$ in subfigure (b). ....	32
Figure 4.11.	Resonant behaviors are almost completely suppressed when the indirect dissipation path is disrupted by severing the odorant-environment connection ( $\chi_v \rightarrow 0$ ). Here, the rate is largely independent of odorant vibrational frequency $f_0$ and is determined solely by the strength of direct dissipation $\chi_e$ . ET rate increases with increasing direct electron-environment coupling $\chi_e$ . ....	34
Figure 4.12.	The direct electron-environment dissipation path drives an exponential relaxation with time constant $T_e$ . Here, $T_e = 33$ fs, and electron+odorant total energy $E(t)$ matches an exponential fit $f_E(t)$ . ....	35

Figure 4.13. As the strength of direct coupling is increased ( $\xi$  decreases), the resonant peaks broaden, and spectroscopic behaviors in the ET rate become masked. .... 36

Figure 4.14. Spectroscopic effects in power dissipation are masked with increasing direct-path dissipation (decreasing  $\xi$ ) for receptors tuned to a specific isotopomer. Subfigure (a) is for a receptor tuned to the C-D stretch frequency, and (b) is for a receptor tuned to the C-H stretch frequency. .... 37

## LIST OF TABLES

Table 3.1.	Physically-interesting values of model parameters are chosen in following with treatments from the literature and are enumerated here [2, 3]. .....	16
Table 4.1.	Power dissipation from the receptor-odorant complex to the environment is enhanced when a ligand is present for which the receptor is tuned (i.e., $\Delta = \hbar\omega_o$ ). When the preferred ligand is replaced by its relative isotopomer, then, $\Delta \neq \hbar\omega_o$ , and power dissipation is suppressed by $\sim 15.4$ dB. This frequency-selective dissipation is used to quantify the selectivity of the receptor to a particular vibrational mode. Here, indirect coupling, $\chi_v = 1/2$ . .....	33
Table 4.2.	In analogy to Table 4.1, receptor selectivity is calculated and tabulated for stronger odorant-environment coupling ( $\chi_v = 2$ ). Increased odorant-environment coupling broadens the resonant peaks in power, reducing receptor selectivity to $\sim 5$ dB (compare to Table 4.1). .....	33
Table 4.3.	Strengthening the direct electron-environment dissipation path (i.e., decreasing $\xi$ ) degrades the sensitivity of a receptor tuned to the C-D stretch frequency. Here, $\chi_v = 1/2$ . .....	38
Table 4.4.	Strengthening the direct electron-environment dissipation path (i.e., decreasing $\xi$ ) degrades the sensitivity of a receptor tuned to the C-H stretch frequency. Here, $\chi_v = 1/2$ . .....	38

## ACKNOWLEDGMENTS

Firstly I would like to express my special appreciation and gratitude to Dr. Enrique P. Blair, my advisor, for having faith and confidence in me. His continuous guidance, motivation, patience, and immense knowledge helped me in all the time of research and writing of this thesis. I can't thank him enough for always being willing to meet me whenever I barged into his office.

Besides my advisor, I would like to thank the rest of my thesis committee for letting my defense be an enjoyable moment. I gratefully acknowledge their time and valuable feedback on this thesis. In particular, I thank Dr. Kevin L. Shuford for his insightful ideas which helped me develop a broader perspective to my thesis. I owe a debt of gratitude to Dr. Linda J. Olafsen for her careful attention to detail.

My sincere thanks goes to my wonderful labmates: Jackson, Joe and Shenghyang, for all the interesting and stimulating discussions we had in the last two years. A very special gratitude goes to Mrs. Minnie Simcik, our Graduate Program Coordinator who kept me organized all the way along and was always ready to help.

I am grateful to my mom, dad, brother and in-laws for their unconditional love, encouragement, and sacrifices. Without them, I would not have made it this far. I also thank my friends: Tazin, Onnesha and Shihab with whom I have shared moments of deep anxiety but also of big excitement. To Jessane, Nazifa and Ben, I will never forget all the great times that we have shared. Life is beautiful with you around.

And, I have saved this last word of acknowledgment for my dear husband - my soulmate: for his love, his patience and his faith, because he always understood.

## DEDICATION

To my life-coach, my father: Because I owe it all to you

## CHAPTER ONE

### Introduction

Much insight into the mechanisms of other senses has been developed, but mysteries persist in our modern understanding of olfaction. It is known that odorant molecules interact with olfactory receptors on sensory neurons, and that an odorant's structure is important in determining its scent, but there is evidence that additional, presently-unknown information may be required to distinguish molecules. For example, isotopomers—molecules related by interchanging some atoms with isotopes—are nearly identical, yet some behavioral experiments suggest that humans and fruit flies can distinguish between isotopomers by smell [4, 5, 6, 7, 8, 9]. Still, the dispute remains unresolved: *in vitro* work also performed in selected mammalian olfactory receptors has not demonstrated a distinguishable response to isotopomer molecules [7], but neurophysiological research has shown that insect antennae can produce a differential response to some isotopomers [10, 11].

Olfactory models may be divided into two broad categories. One category may be termed “lock-and-key” models, or “odotope” models, in which odorant structure alone is assumed to determine the receptor response, just as a key's shape determines whether it can actuate a lock. A second class of models known as “swipe-card” models extend the lock-and-key model in that structure is recognized as necessary but insufficient to distinguish odors [12]. One prominent swipe-card theory invokes quantum mechanics: a suitable structure *and* additional information encoded in the molecule trigger the olfactory response. This is in analogy to a magnetic hotel key card, which must not only fit in the swipe-card slot, but also must have the proper keyword encoded in the magnetic strip.

Turin posited that spectroscopic information about a molecule could enhance an electron transfer (ET) rate, which would play an integral role in distinguishing between odorants [13, 14]. After entering the nasal cavity and diffusing through the mucus layer, an odorant molecule may dock with an odorant receptor, a large protein spanning the bilipid cellular membrane. Here, the receptor is prepared with an electron on an donor site  $D$  (electronic state  $|D\rangle$ , at an energy  $E_D$ ). This is illustrated in the left-most portion of Figure 1.1. Detection involves ET to an acceptor site  $A$ , at energy  $E_A$ , which is  $\Delta$  below  $E_D$ . A direct  $|D\rangle \rightarrow |A\rangle$  transition does not conserve energy, and thus is unlikely. On the other hand, if an odorant vibrational mode has quantization  $\hbar\omega_o = \Delta$ , then an inelastic  $|D\rangle \rightarrow |A\rangle$  ET may readily occur with the associated excitation of a quantum of vibration in the odorant. A frequency-selective response of this type is referred to as inelastic electron tunneling spectroscopy (IETS), and an olfactory IETS process is depicted in the center part of Figure 1.1. Then, the transferred electron is presumed to trigger some subsequent process, which continues the chain of events in sensing (in Figure 1.1, this ET triggers the activation of the G protein, which releases an  $\alpha$  subunit).

In this work, we focus on the  $|D\rangle \rightarrow |A\rangle$  transition without considering downstream and upstream events in the sequence leading to an olfactory detection. A fully-quantum, numerical model of the vibration-coupled IETS mechanism is modeled here.

Indeed, previous models of the vibrational theory of olfaction exist. Some of these models obtain an ET rate through Fermi's golden rule and are semi-classical in the sense that the electronic component is given a quantum treatment, and the vibrational components are treated classically [2, 15]. Other models go beyond Fermi's golden rule and get an ET rate from a master equation that includes the spectrum of the odorant and environmental harmonic oscillators [16, 17, 18, 19]. Here the system is partitioned such that the degrees of freedom of the oscillators are traced over in the

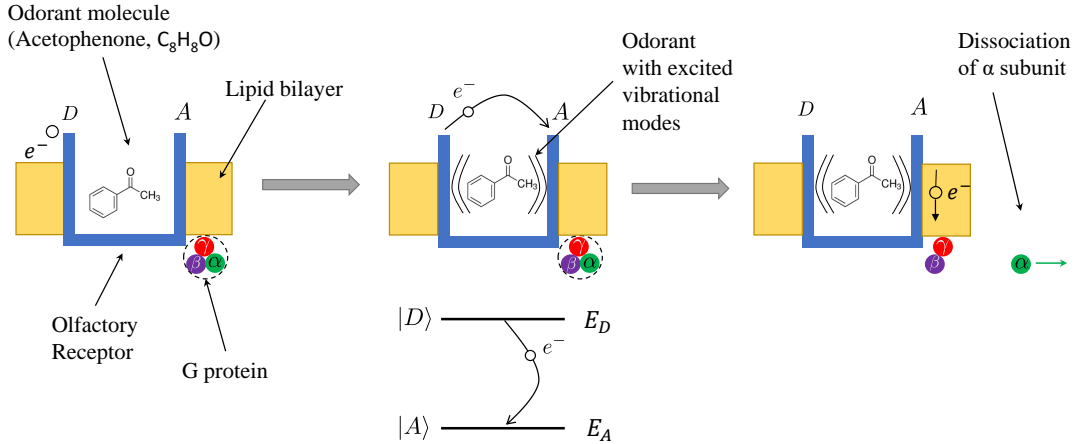


Figure 1.1: The inelastic electron tunneling spectroscopy (IETS) mechanism is illustrated in the context of human olfaction. A human odorant receptor is known to be a G-protein coupled receptor (GPCR, shown in blue, with an associated G protein). When an odorant molecule docks in the receptor (left figure), an electron transition from  $D$  (quantum state  $|D\rangle$ ) at energy  $E_D$  to  $A$  (state  $|A\rangle$ ) at energy  $E_A$  requires a change in energy that is facilitated by the excitation of a quantum of molecular vibrational energy. Once complete, the transferred electron may trigger the activation of the associated G protein, leading to an action potential and a sensory detection event. Without an odorant having a properly-quantized vibrational spectrum, the electron transition and subsequent detection are much less probable.

development of the master equation. In one of these models, the dissipation of energy (or power) was found to enhance a receptor's selectivity for a particular vibrational quantization in an odorant [17]. Another such model of chiral odorants showed that an energy difference between the ground states of enantiomer pairs could also lead to a rate-based dissipative discriminatory mechanism [20]. While other models treat vibrational modes of the odorant and the environment as part of the reservoir and trace over these degrees of freedom to obtain a master equation, we develop a non-equilibrium model in which both the electron transfer and the dominant odorant vibrational mode are treated explicitly. This model lends itself to a calculation of power dissipation and highlights the link between power dissipation and electron transfer.

## CHAPTER TWO

### Background

#### *Overview of the Olfactory Process*

The human olfactory process is depicted in Figure 2.1. It begins with the inhalation of an odorant molecule into the nasal cavity, where the odorant must diffuse through a mucus layer before arriving at the olfactory epithelium for a potential detection. Inside the mucus layer, the odorant encounters odorant-binding proteins, and it may also be modified by biotransformation or detoxification enzymes [21]. The odorant-binding proteins may enhance the diffusion of hydrophobic odorants across the mucus layer to the olfactory epithelium. The biotransformation enzymes could prevent certain molecules from reaching the olfactory receptor.

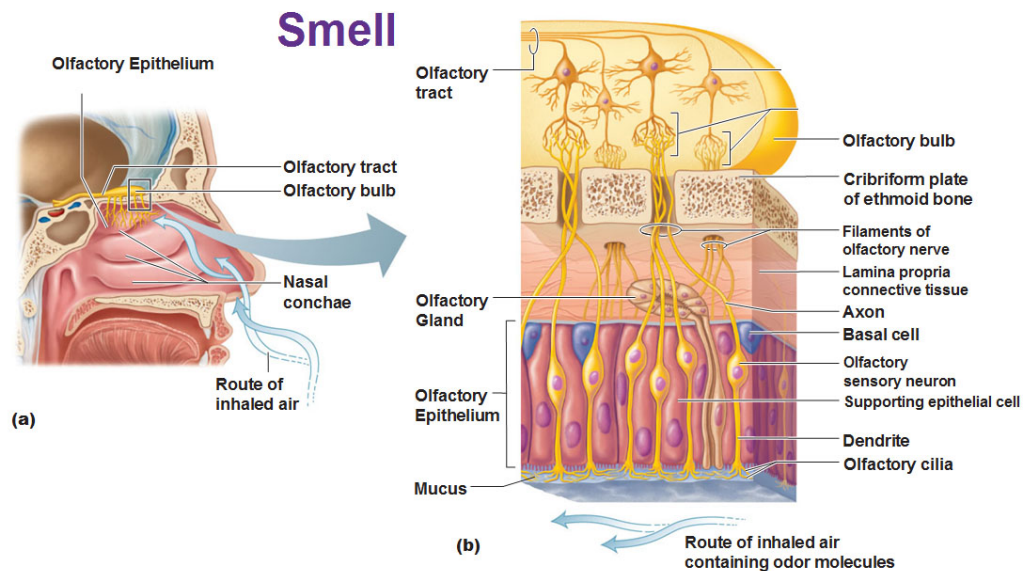


Figure 2.1: An overview of the olfactory process in humans. Odorant molecules enter the nasal cavity and approach the olfactory epithelium [frame (a)]. Odorants must diffuse through a mucus layer prior to reaching the olfactory epithelium [frame (b)]. At the epithelium, odorants must interact with olfactory receptors on the olfactory cilia projecting from the olfactory sensory neuron's dendritic process [1].

Only after diffusing through the mucus layer can the odorant contact an olfactory receptor on the cilia projecting from the dendritic process of an olfactory sensory neuron. If this odorant can trigger an appropriate response from the olfactory receptor, an action potential is generated within the sensory neuron's cilia, and an electrochemical response is transmitted via the neuron's axon to the olfactory bulb, where it is received and transmitted to the brain as an olfactory signal [12, 21, 22]. The interaction between the olfactory receptor and the odorant molecule is the least understood part of this chain of events and is the focus of this work: perireceptor and neuronal processes are not addressed here.

### *Cases Inexplicable by Structural Models*

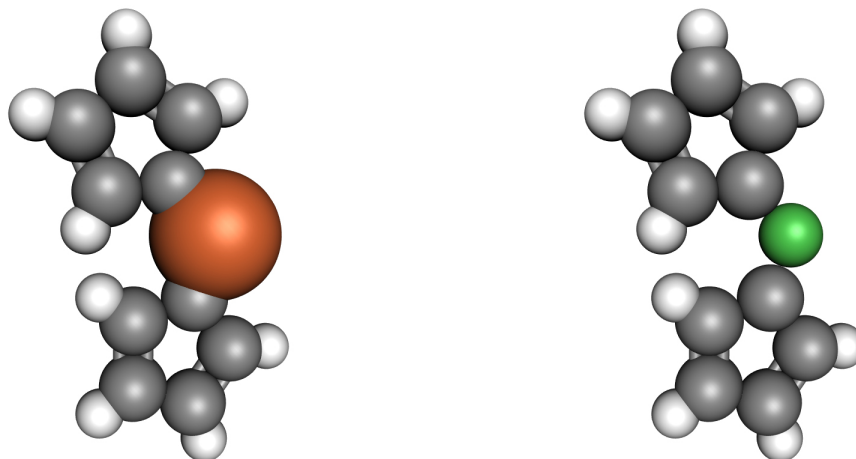
The structure-based mechanism suitably describes many receptors, and it likely works for olfactory receptors specific to a particular molecule. However, there are some cases which structural models do not explain well, of which some are listed:

#### *Structurally-Similar Odorants which Smell Differently*

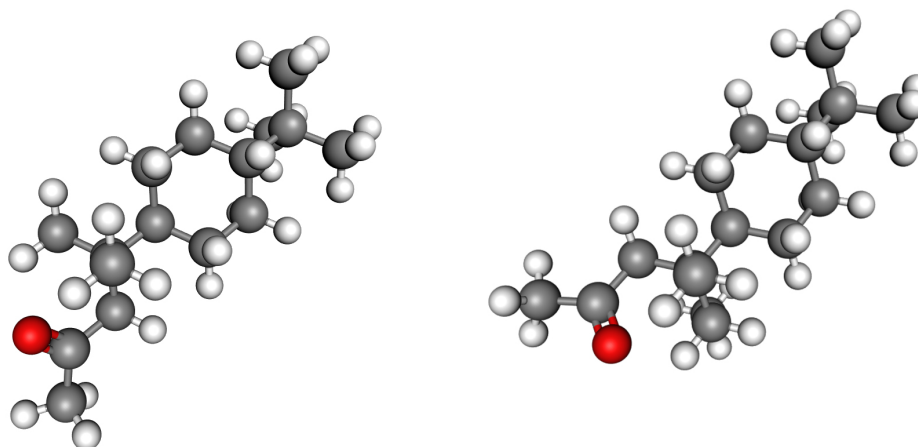
Some odorants with similar structure smell differently. For example, Nickelocene,  $\text{Ni}(\text{C}_5\text{H}_5)_2$  and Ferrocene,  $\text{Fe}(\text{C}_5\text{H}_5)_2$  appear to have the same structure, but the former is said to have smell of "oily-chemical," and the latter to smell "spicy" [13]. Cis-nor-ketone and Cis-ketone is very similar in structure but Cis-nor-ketone is nearly odorless and Cis-ketone are said to have a "penetrating urine odor" [12]. See Figure 2.2.

#### *Molecules with Different Structures but Similar Odors*

Molecules with different structures but similar odors are equally inexplicable by lock-and-key models. Both 5a-androst-16-en-3-one and cis-ketone are said to have a "penetrating urine odor" but their structures are different [12].



(a) 3D models of ferrocene (left) and nickelocene (right).



(b) Cis-nor-ketone (left) and cis-ketone (right).

Figure 2.2: (a) Ferrocene,  $\text{Fe}(\text{C}_5\text{H}_5)_2$  and nickelocene,  $\text{Ni}(\text{C}_5\text{H}_5)_2$  have very similar structures but have distinctly different scents. (b) Cis-nor-ketone (4-(4-tert-butylcyclohexyl)-4-methylpentan-2-one) and cis-ketone (4-(4-tert-butylcyclohexyl)-4-methylhexan-2-one) are very similar in structure but the former is said to be nearly odorless and the latter is said to have a “penetrating urine odor”.

### Isotopomers

An isotopomer is formed by substituting an isotope for an atom in a commonly-occurring molecule. Such isoforms are very nearly structurally and electronically identical (see Figure 2.3).

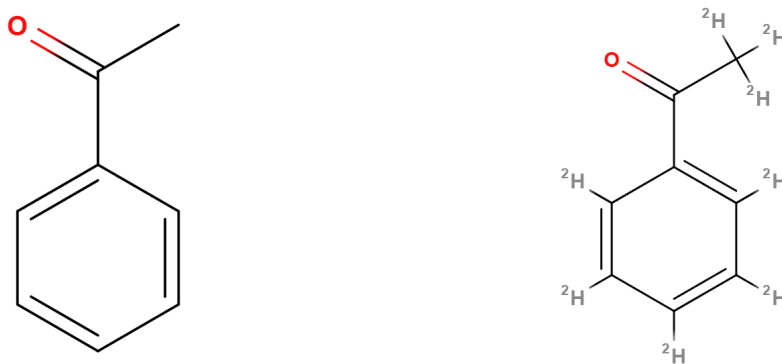


Figure 2.3: Commonly-occurring acetophenone (ACP-h) (left) and its fully-deuterated isotopomer acetophenone-d8 (ACP-d)(right). They are structurally and electronically very similar.

The results of behavioral studies conflict on whether humans and fruit flies can distinguish common benzaldehyde from deuterated isotopomers, or acetophenone from deuterated isotopomers [4, 5, 15, 16, 23]. A recent *in vitro* study showed no differentiable response to isoforms in selected human and mouse olfactory receptors [7]. However, commonly-occurring acetophenone (ACP-h) and its fully-deuterated isotopomers, such as acetophenone-d8 (ACP-d) resulted in quantifiably different neurophysiological responses in the antenna lobe of honeybees. Each isoform leads to a different activation pattern in the clusters of nerve endings known as glomeruli at the base of the antenna [10, 11]. No study has yet eliminated perireceptor events, such as interaction with odorant-binding proteins or detoxification enzymes, which help distinguish one isotopomer from another, and it must be recognized that insect olfactory receptors are not identical to those found in mammals.

### *Motivation for the Vibrational Theory of Olfaction*

Inexplicable cases such as mentioned in the previous section motivate the need for another type of olfactory theory - the vibrational theory of olfaction which is a swipe-card model. The vibrational theory of olfaction posits that quantized molecular vibrations provide the discriminating information needed by an olfactory receptor in addition to odorant's molecular structure. Dyson initially suggested this concept in 1938 [24], and Turin suggested that inelastic tunneling spectroscopy (IETS) could be the mechanism behind the vibrational discrimination of odorants [13]. Overview of the IETS mechanism in vibrational theory of olfaction is illustrated in Figure 1.1.

### *Existing Semi-classical Models for the Vibrational Theory of Olfaction*

Existing quantitative models of the vibrational theory of olfaction are semi-classical, relying on Fermi's Golden Rule. An example of a semiclassical model is described here, which was developed by Brookes, *et al.* [2, 12]. This model has three components: the electronic system, an odorant molecule, and a bath. The electronic system is a two-state system with configurations  $|D\rangle$  (electron on the donor) and  $|A\rangle$  (electron on the acceptor). The odorant molecule is treated as a harmonic oscillator with Hamiltonian

$$\hat{H}_o = \hbar\omega_o \left( \hat{a}^\dagger \hat{a} + \frac{1}{2} \right) \quad (2.1)$$

where  $\omega_o$  is the characteristic angular frequency of the single dominant odorant vibrational mode to which the electron transfer is coupled, and  $\hat{a}^\dagger$  and  $\hat{a}$  are the creation and annihilation operators for the vibrational mode. The eigenstates  $\{|n\rangle\}$  of this vibrational mode satisfy the time-independent Schrödinger equation

$$\hat{H}_o |n\rangle = E_n |n\rangle \quad (2.2)$$

and provide a convenient basis for the system. The bath is modeled as a system of harmonic oscillators, each with characteristic angular frequency  $\omega_q$  and raising and

lowering operators,  $\hat{a}_q^\dagger$  and  $\hat{a}_q$ . The Hamiltonian for the bath is given by

$$\hat{H}_{env} = \sum_q \hbar\omega_q \left( \hat{a}_q^\dagger \hat{a}_q + \frac{1}{2} \right) \quad (2.3)$$

A convenient basis for this system is  $\{|N\rangle = |n_1, n_2, n_3, \dots\rangle\}$ , the set of states formed by taking products of the eigenstates of individual environmental oscillators.

These three components are linked and described by the global Hamiltonian

$$\hat{H} = \hat{H}_D + \hat{H}_A + \hat{v} \quad (2.4)$$

where  $\hat{v}$  captures the energetics of the transition between the electronic states  $\hat{v} = t(|D\rangle\langle A| + |A\rangle\langle D|)$ , and  $\hat{H}_X$ , with  $X \in \{D, A\}$ , captures the coupling between the electronic state  $|X\rangle$  and the odorant and environment:

$$\hat{H}_X = |X\rangle\langle X| (\epsilon_X + \hat{H}_{osc} + \hat{H}_{e-osc,X}) \quad (2.5)$$

Here,  $\hat{H}_{osc} = \hat{H}_o + \hat{H}_{env}$  describes the odorant and the bath. The coupling between the electronic state  $|X\rangle$  and the odorant+bath composite is given by

$$\hat{H}_{e-osc,X} = \gamma_X (\hat{a} + \hat{a}^\dagger) + \sum_q \gamma_{qX} (\hat{a}_q + \hat{a}_q^\dagger) \quad (2.6)$$

Here,  $\gamma_X$  is the coupling constant between state  $|X\rangle$  and the odorant, and  $\gamma_{qX}$  couples  $|X\rangle$  to the  $q^{th}$  oscillator. The composite states  $\{|XnN\rangle\}$  are products of the unperturbed eigenstates of the individual subsystems. The eigenstates of  $\hat{H}_X$  are given by

$$|\Psi_{XnN}\rangle = \exp \left[ u_X (\hat{a} - \hat{a}^\dagger) + \sum_q u_{qX} (\hat{a}_q - \hat{a}_q^\dagger) \right] |XnN\rangle \quad (2.7)$$

The eigenvalues are

$$E_{XnN} = \epsilon_X + \left( n + \frac{1}{2} - u_X^2 \right) \hbar\omega_o + \sum_q \left( n_q + \frac{1}{2} u_{qX}^2 \right) \hbar\omega_q \quad (2.8)$$

Here,  $u_X = \gamma_X / \hbar\omega_o$ , and  $u_{qX} = \gamma_{qX} / \hbar\omega_q$ . A characteristic time  $\tau_{Tn}$  may be obtained for a  $|D0\rangle \rightarrow |An\rangle$  transition. This is a transition from a state with the electron on  $D$  and the odorant in its ground state ( $|D0\rangle$ ) to another configuration with the electron

on  $A$  and the odorant in the  $n^{\text{th}}$  excited state ( $|An\rangle$ ). From Fermi's Golden Rule,

$$\frac{1}{\tau_{Tn}} = \frac{2\pi}{\hbar} \sum_{N,N'} P_N |\langle \Psi_{D0N} | \hat{v} | \Psi_{AnN'} \rangle|^2 \quad (2.9)$$

where  $P_N$  is the probability that the environment starts in state  $|D0N\rangle$ . Standard approximations for an electron coupled to a bath of phonons and the assumption that background fluctuations are of low frequency lead to a Marcus-type expression:

$$\frac{1}{\tau_{Tn}} = \frac{2\pi}{\hbar} t^2 \frac{\sigma_n}{\sqrt{4\pi k_B T \lambda}} \exp\left(-\frac{(\epsilon_n - \lambda)^2}{4k_B T \lambda}\right) \quad (2.10)$$

where  $\sigma_n = \exp(-S) S^n / n!$ ,  $S = (u_D - u_A)^2$  (a Huang-Rhys factor),  $\epsilon_n = \epsilon_D - \epsilon_A - n\hbar\omega_o$ ,  $\lambda = \sum_q S_q \hbar\omega_q$  (reorganization energy), and  $S_q = (u_{qD} - u_{qA})^2$ . Also,  $k_B$  is the Boltzmann constant, and  $T$  is temperature. At this point, the model has become semi-classical: the odorant and environmental oscillators now are treated classically, while the electronic model remains quantum mechanical. Within this model, IETS-based odorant discrimination requires the inelastic tunneling event to be much more likely than an elastic transition. The inelastic transition begins with configuration  $|D0\rangle$  and results in  $|A1\rangle$  (the electron on the acceptor and the vibrational system in the first excited state). This is characterized by time  $\tau_{T1}$ . The elastic transition, however, leaves the odorant unexcited, resulting in final state  $|A0\rangle$  with characteristic time  $\tau_{T0}$ . In terms of the characteristic times, for the elastic process  $|D0\rangle \rightarrow |A1\rangle$  to be a more likely transition than the elastic process  $|D0\rangle \rightarrow |A0\rangle$ , the relationship  $\tau_{T1} \ll \tau_{T0}$  should be satisfied. Under these conditions, we say that the inelastic process dominates the elastic process. To assess whether it is plausible for the inelastic process to dominate in this model, typical parameters are chosen. Since little is known about the D and A sites, some reasoning must be applied to obtain receptor parameters. An effective hopping integral  $\gamma = 1$  meV, Temperature  $T = 300\text{K}$ ,  $\hbar\omega_o = 200$  meV is chosen and a receptor tuned to this frequency would have  $\epsilon_D - \epsilon_A = \hbar\omega_o$ . With these parameters,  $\tau_{T0} \sim 87$  ns and  $\tau_{T1} \sim 1.3$  ns, satisfying  $\tau_{T1} \ll \tau_{T0}$ , and the inelastic process does in fact dominate the elastic process. However, for  $\lambda > \sim 60$  meV,  $\tau_{T1}$  no

longer dominates  $\tau_{T0}$ , and the semi-classical model predicts that IET can no longer be a discriminating factor in this region of the parameter space. Additionally, it has been argued that  $\lambda = 30$  meV is unusually low, and should be an order of magnitude larger to be realistic [7]. By this argument, the vibrational theory of olfaction is implausible for more reasonable system parameters.

For the fully-quantum model explained here, this is not an issue. It must be noted that olfactory IETS is quantum mechanical, but it is being treated in a semi-classical limit. In the next section, a fully-quantum model for Olfactory IETS is presented.

## CHAPTER THREE

### Model

#### *Framework*

The framework for this fully-quantum model of the vibrational theory of olfaction is an electronic two-state system dissipatively coupled in two ways to the thermal environment: (1) a direct coupling to environmental degrees of freedom, and (2) an indirect coupling via environmentally-damped odorant vibrations. The dynamics of the electronic system and one dominant odorant vibrational mode are explicitly treated in this work. Dissipative effects are driven by interactions with the total environment, which is not explicitly modeled here but may include receptor vibrations and solvent degrees of freedom. The indirect dissipative path gives rise to spectroscopic behavior and is modeled using damped quantum oscillators to treat odorant vibrational modes. The direct electron-environment dissipation path is treated by building electronic relaxation into the model. This is depicted schematically in Figure 3.1. For computational tractability, only one odorant vibrational mode is presumed to be strongly dominant (the coupling between the electron and all other odorant modes is ignored).

The electronic state is described by the Hamiltonian  $\hat{H}_e = (\Delta/2)\hat{\sigma}_z - \gamma\hat{\sigma}_x$ , where  $\hat{\sigma}_x$  and  $\hat{\sigma}_z$  are Pauli operators, which we may write in terms of transition operators  $\hat{P}_{jk} \equiv |j\rangle\langle k|$  and projection operators  $\hat{P}_j \equiv |j\rangle\langle j|$ :  $\hat{\sigma}_x = \hat{P}_{AD} + \hat{P}_{DA}$  and  $\hat{\sigma}_z = \hat{P}_D - \hat{P}_A$ . The parameter  $\gamma$  is the hopping energy between the two states  $|D\rangle$  and  $|A\rangle$ , also known as the coupling constant,  $H_{AB}$ , in quantum chemistry. The detuning between the two states,  $\Delta$ , functions as the driving force behind the electron transfer:  $\Delta = E_D - E_A$ .

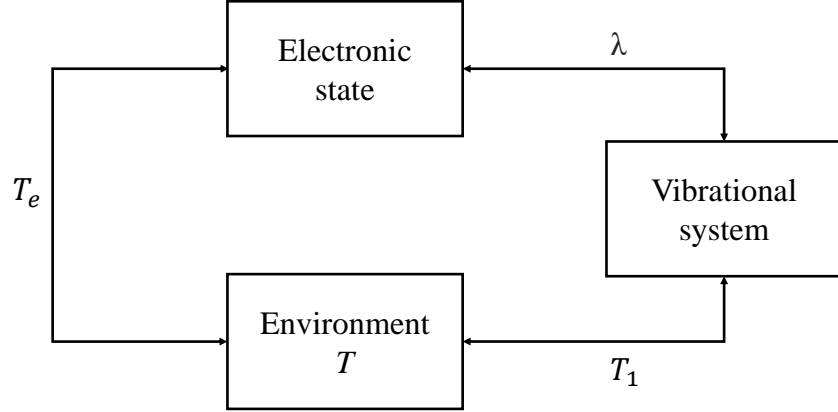


Figure 3.1: The model developed in this paper includes the explicit, fully-quantum treatment of a  $|D\rangle \rightarrow |A\rangle$  electron transfer event (ET) coupled to a dominant odorant vibrational mode. The “Electronic state” represents the ET event, and the “Vibrational system” represents the dominant odorant mode. This ET event is coupled to the thermal environment both directly, and indirectly via the odorant vibrational mode. In each case, the parameter that characterizes coupling between two systems is listed.

The dominant odorant vibrational mode is modeled as a quantum harmonic oscillator, with Hamiltonian  $\hat{H}_v$ :

$$\hat{H}_v = \left( \hat{a}^\dagger \hat{a} + \frac{1}{2} \right) \hbar \omega_o = \frac{\hat{P}^2}{2m_o} + \frac{1}{2} m_o \omega_o^2 \hat{Q}^2. \quad (3.1)$$

Here,  $\omega_o$  is the frequency of the dominant oscillator mode;  $\hbar$  is the reduced Planck constant; and  $m_o$  is the dominant vibrational mode’s effective mass. The position (coordinate) operator  $\hat{Q}$  and the momentum operator  $\hat{P}$  may be written in terms of  $\hat{a}^\dagger$  and  $\hat{a}$ , the creation and annihilation operators, respectively:

$$\hat{Q} = \sqrt{\frac{\hbar}{2m_o\omega_o}} (\hat{a}^\dagger + \hat{a}) \quad \text{and} \quad \hat{P} = i\sqrt{\frac{m_o\omega_o\hbar}{2}} (\hat{a}^\dagger - \hat{a}). \quad (3.2)$$

The right-hand side of Eqn. (3.1) is written in terms of the kinetic energy ( $\hat{P}^2/2m_o$ ) and the potential energy ( $m_o\omega_o^2\hat{Q}^2/2$ ) operators for this vibrational mode.

The coupling between the odorant and the receptor’s electronic state is described by a linear coupling term in the Hamiltonian,

$$\hat{H}_{ev} = \frac{g_{ev}}{2} \hat{\sigma}_z \hat{Q}. \quad (3.3)$$

The coupling constant  $g_{ev}$  depends on  $\lambda$ , the reorganization energy of the odorant's dominant vibrational mode:  $g_{ev} = \sqrt{m_o \omega_o^2 \lambda}$ . Thus, the fully-quantum system is described by the total Hamiltonian,  $\hat{H}$ , given by

$$\begin{aligned} \hat{H} &= \hat{H}_e + \hat{H}_v + \hat{H}_{ev} \\ &= \frac{\Delta}{2} \hat{\sigma}_z - \gamma \hat{\sigma}_x + \frac{\hat{P}^2}{2m_o} + \frac{1}{2} m_o \omega_o^2 \hat{Q}^2 + \frac{g_{ev}}{2} \hat{\sigma}_z \hat{Q}. \end{aligned} \quad (3.4)$$

The effects of the bath on the electron+odorant system may be modeled by treating it as an open quantum system in a Markovian environment. To do this, we use the Lindblad equation [25],

$$\frac{d}{dt} \hat{\rho} = -\frac{i}{\hbar} [\hat{H}, \hat{\rho}] + \mathfrak{D}. \quad (3.5)$$

The density operator,  $\hat{\rho}(t)$ , describes the time-dependent state of the electron+odorant system. The first term describes unitary dynamics and is equivalent to the quantum Liouville equation. The dissipator,  $\mathfrak{D}$ , models environmental effects and is given by

$$\mathfrak{D} = \sum_{j=1}^s \hat{L}_j \hat{\rho} \hat{L}_j^\dagger - \frac{1}{2} \{ \hat{L}_j^\dagger \hat{L}_j, \hat{\rho} \}. \quad (3.6)$$

The Lindblad operators,  $\{\hat{L}_j\}$ , also known as environmental channels, describe the effects of the environment on the odorant-receptor complex. In this model, the indirect-path Lindblad operators are chosen so as to damp only the vibrational subsystem. In particular, two Lindblad operators will be used:

$$\hat{L}_1 = \frac{1}{\sqrt{T_1}} \hat{a}, \quad \text{and} \quad \hat{L}_2 = \exp\left(-\frac{\hbar \omega_o}{2k_B T}\right) \frac{1}{\sqrt{T_1}} \hat{a}^\dagger. \quad (3.7)$$

The operator  $\hat{L}_1$  removes energy from the vibrational system, with  $T_1$  being a phenomenological characteristic time for exponential energy relaxation via this indirect path. After a time  $t \gg T_1$ , the system will relax to its ground state if only  $\hat{L}_1$  is used. The operator  $\hat{L}_2$  excites the system and includes a prefactor which depends on temperature  $T$ . When both  $\hat{L}_1$  and  $\hat{L}_2$  are used in concert, they drive the system to a Boltzmann distribution. Finally, the direct electron-environment coupling is modeled

using an additional pair of Lindblad operators,  $\hat{L}_3$  and  $\hat{L}_4$ , given by:

$$\hat{L}_3 = \frac{1}{\sqrt{T_e}} \hat{P}_{DA}, \quad \text{and} \quad \hat{L}_4 = \exp\left(-\frac{\Delta}{2k_B T}\right) \frac{1}{\sqrt{T_e}} \hat{P}_{AD}. \quad (3.8)$$

Here,  $T_e$  is the characteristic time for an exponential relaxation via the direct electron-environment dissipation path. The combination of  $\hat{L}_3$  and  $\hat{L}_4$  drives the system to a Boltzmann distribution.

To quantify the strength of environmental coupling, it is helpful to define coupling strength ratios. For indirect coupling, the harmonic oscillator's period  $T_o = 2\pi/\omega_o$  is the natural time scale, so  $\chi_v \equiv T_o/T_1$  provides a useful measure of vibron-environment coupling. A vibrational system decoupled from the environment is characterized by  $\chi_v \rightarrow 0$ . For the electronic system, the detuning,  $\Delta$ , is the natural energy scale, so we use  $\chi_e \equiv t_\Delta/T_e$  to characterize the strength of direct electron-environment coupling, where  $t_\Delta \equiv \hbar/\Delta$ . Small  $\chi_e$  characterizes an electronic system for which direct environmental dissipation is suppressed. Additionally, when comparing the two coupling strengths, we use the ratio  $\xi \equiv T_e/T_1$ , for which  $\xi \rightarrow 0$  when direct electron-environment coupling is dominant, and  $\xi \rightarrow \infty$  for dominant indirect electron-environment coupling via the odorant vibrational mode.

In order to qualitatively show that in the regime of interest, the fully-quantum model is preferable over a semi-classical treatment, we reduce the fully-quantum model to a semi-classical treatment. If the kinetic energy of the oscillator is ignored, and if the coordinate is treated as a classical variable instead of as an operator ( $\hat{Q} \rightarrow Q$ ), then the Hamiltonian reduces to a Marcus-type Hamiltonian,  $\hat{H}^{(M)}$ , which acts on the Hilbert space of the electronic system only:

$$\hat{H}^{(M)} = \frac{\Delta}{2} \hat{\sigma}_z - \gamma \hat{\sigma}_x + \frac{1}{2} g_{ev} \hat{\sigma}_x Q^2 + \frac{1}{2} m_o \omega_o^2 Q^2. \quad (3.9)$$

### *Choice of Parameters*

In the absence of concrete experimental data for model parameters, we pick typical values for biological systems and theorized values from the literature. Thus, all calculations are performed at ambient temperature ( $T = 293$  K) unless the role of temperature is investigated. A tunneling energy  $\gamma = 1$  meV is chosen, in following with analysis found in the literature [2].  $D$  and  $A$  are treated as single molecular orbitals coupled to each other by a weak hopping integral  $\gamma$ , as there should be essentially no tunneling from  $D$  to  $A$  in the absence of the odorant or any other dissipative pathway. We often use a  $D$ - $A$  detuning of  $\Delta \sim 200$  meV ( $1613.6$  cm $^{-1}$ ), chosen since the interesting range in olfaction is  $70$  meV  $< \hbar\omega_o < 400$  meV ( $564.77$  cm $^{-1} < \hbar\omega_o < 3227.3$  cm $^{-1}$ ) [2, 3]. The odorant reorganization energy is varied between  $30$  meV ( $\sim k_B T$  at biological temperatures) and  $300$  meV ( $\sim \Delta$ ). Table 3.1 contains the chosen model parameters.

Table 3.1: Physically-interesting values of model parameters are chosen in following with treatments from the literature and are enumerated here [2, 3].

Parameter	Value
$\Delta$	200 meV ( $1613.6$ cm $^{-1}$ )
$\gamma$	1 meV
$\lambda$	30-300 meV
$T$	293 K

### *Justification for a Fully-quantum Treatment*

A comparison of the statics between the fully-quantum treatment and the semi-classical Marcus-type reduction reveals the necessity for a fully-quantum treatment of IETS within this model. The stationary states  $|\phi_k\rangle$  and eigenvalues  $E_k$  for the Hamiltonian of Eqn. (3.4) are found by solving the time-independent Schrödinger equation:

$$\hat{H} |\phi_k\rangle = E_k |\phi_k\rangle \tag{3.10}$$

The semiclassical  $\hat{H}^{(M)}$  has two eigenstates,  $\{|\phi_k^{(M)}\rangle\}$ , with  $k \in 1, 2$ , and two eigenvalues  $V_k^{(M)}$ , which solve the time-independent Schrödinger equation:

$$\hat{H}^{(M)} |\phi_k^{(M)}\rangle = V_k^{(M)} |\phi_k^{(M)}\rangle \quad (3.11)$$

Since  $\hat{H}^{(M)}$  is a function of the coordinate  $Q$ , so also are the eigenvalues  $V_k^{(M)}(Q)$  and eigenstates  $|\phi_k^{(M)}(Q)\rangle$ . The eigenvalues  $V_k^{(M)}(Q)$  provide an adiabatic potential-energy landscape for the semi-classical system. Figure 3.2 shows the potential energy surfaces defined by the  $\{V_k^{(M)}(Q)\}$  for the semiclassical system, along with the lowest-energy eigenvalues for the fully-quantum system.

The  $\{V_k^{(M)}(Q)\}$  surfaces are plotted with  $Q$  scaled to  $Q_0 = g_{ev}/2m_o\omega_o^2$ . The energy quantization in the fully-quantum treatment is significant compared to the feature sizes seen in the potential landscape of the semi-classical treatment. This indicates that the fully-quantum treatment of the electron+odorant system is justified, indeed. Thus, the fully-quantum treatment will yield results which semi-classical models cannot capture. This comparison is performed for two different values of  $\lambda$ . It is seen that for a larger  $\lambda$ , the potential barrier between the coordinates  $Q = \pm 1$  becomes more significant.

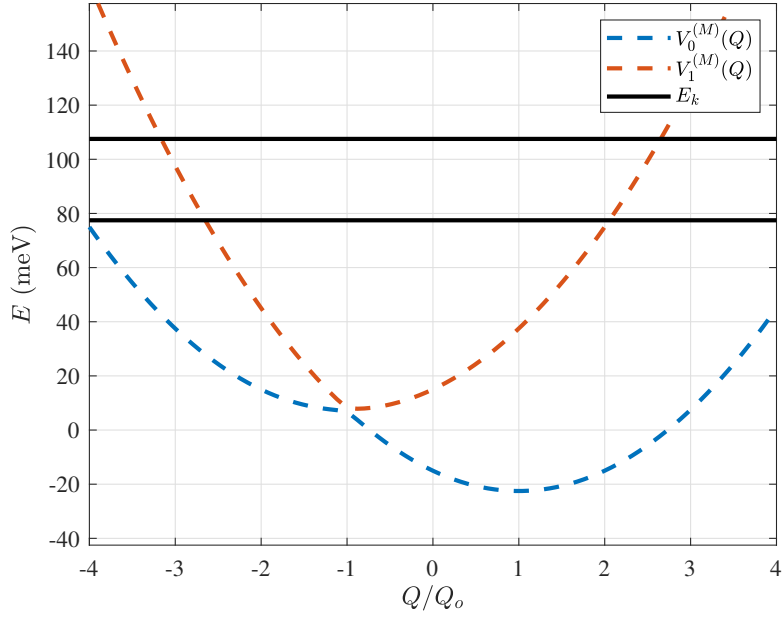
### *Calculation of Electron Transfer Time, $t_{ET}$*

Electron transfer times,  $t_{ET}$ , within the fully-quantum treatment are obtained from the time dynamics of the non-equilibrium model calculations. First, the system is prepared in an initial state  $\hat{\rho}(t \leq 0)$ , which is chosen to be,  $\hat{\rho}_0^{th}$ , the thermal equilibrium density matrix for the electron+ odorant system:

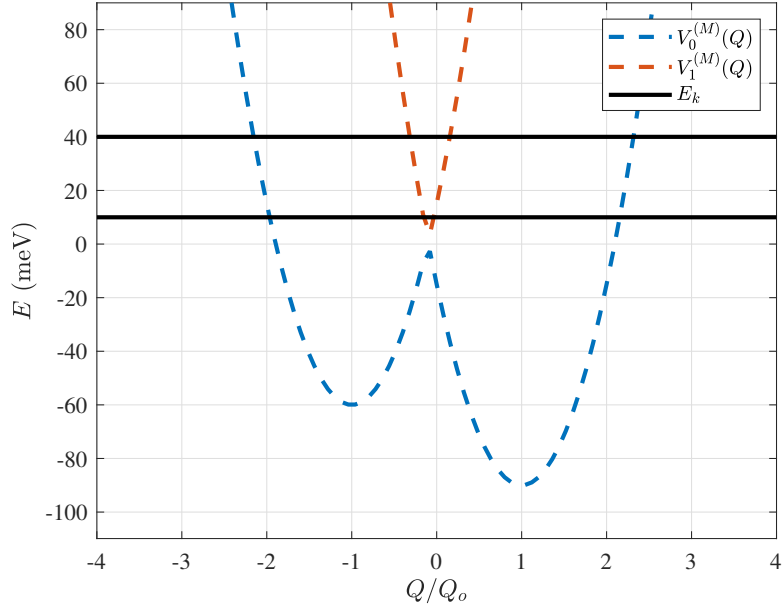
$$\hat{\rho}(0) = \hat{\rho}_0^{th} \equiv \frac{1}{Z} \exp\left(-\frac{1}{k_B T} \hat{H}_0\right),$$

with

$$Z = \text{Tr} \left( \exp\left(-\frac{1}{k_B T} \hat{H}_0\right) \right).$$



(a)  $\lambda = 30$  meV



(b)  $\lambda = 300$  meV

Figure 3.2: A fully-quantum treatment within the vibrational theory of olfaction is justified. The eigenvalues of the fully-quantum Hamiltonian  $\hat{H}$  are plotted relative to the Marcus-type potential energy surfaces  $V_k^{(M)}(Q)$  vs.  $Q$ . This plot is shown for two different values of the odorant reorganization energy  $\lambda$ : once with  $\lambda = 30$  meV and again with  $\lambda = 300$  meV. In each case, the energy discretization of fully-quantum system is significant compared to feature sizes of semi-classical adiabatic Marcus-type potential surfaces. This suggests that treatment using the fully-quantum model will lead to behaviors not captured by a Marcus-type semi-classical model.

Here,  $\hat{H}_0$  is similar to  $\hat{H}$  from Equation (3.4), but differs in that we set  $\Delta(t \leq 0) = \Delta_0$ .  $\Delta_0$  is a large negative potential applied for the sole purpose of confining the electronic state to  $|D\rangle$ . Then, at  $t = 0$ ,  $\Delta(t)$  is changed abruptly to a positive, static value appropriate to the physics of the receptor. Next,  $\hat{\rho}(t)$  is obtained for  $t > 0$  by solving Eqn. (3.5) numerically using the new, constant  $\hat{H}$  for  $t > 0$ , and using  $\hat{\rho}(0)$  as the initial value. The probabilities for finding the electron on the donor site and the acceptor sites,  $P_D$  and  $P_A$ , respectively, are calculated as the expectation value of the projection operators:  $P_D = \langle \hat{P}_D \rangle$  and  $P_A = \langle \hat{P}_A \rangle$ .

Figure 3.3 shows non-equilibrium model data from which an electron transfer time  $t_{ET}$  is calculated.

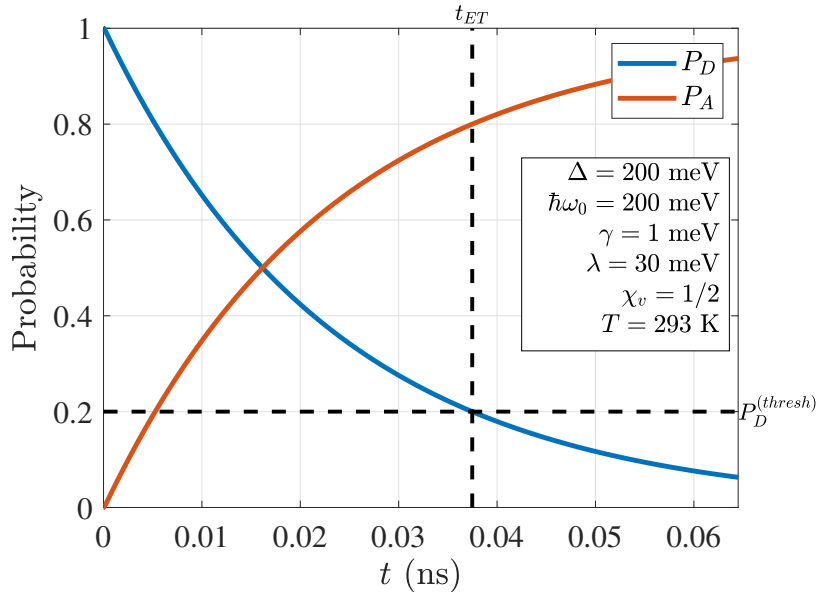


Figure 3.3: Calculation of threshold defined electron transition time,  $t_{ET}$ , from the dynamic solution to Eqn. (3.5). Here,  $\hat{\rho}(t)$  is calculated and the probabilities  $P_D$  and  $P_A$  for finding the electron on  $D$  or  $A$  are calculated.  $t_{ET}$  is defined as the time when  $P_D$  drops from  $P_D(0) \simeq 1$  to a threshold value  $P_D^{(thresh)}$ . When  $P_D^{(thresh)} = 0.2$ , the result is  $t_{ET} = 37.5$  ps. Dashed black lines indicate the threshold  $P_D^{(thresh)} = 0.2$  and the electron-transfer time,  $t = t_{ET}$ , defined as the time that  $P_D$  drops below  $P_D^{(thresh)}$ .

$t_{ET}$  is defined as the time when  $P_D$  drops from  $P_D(0) \simeq 1$  to a threshold value  $P_D^{(thresh)}$ . The electron transfer rate  $k$  is the reciprocal of the electron transfer

time:  $k = 1/t_{ET}$ . While any  $P_D^{(thresh)} < 0.5$  could serve as a threshold, we choose  $P_D^{(thresh)} = 0.2$  because this is low enough to preclude complicating oscillations in  $P_D(t)$  as  $P_D(t) \rightarrow P_D^{(thresh)}$ , and yet high enough to allow reasonable calculation times. This calculation is performed with large  $\xi$  so that indirect dissipation is dominant. Enhancing the direct dissipation pathway (reducing  $\xi$ ) would allow a faster relaxation, resulting in a faster ET and a higher rate  $k$ .

The Rabi oscillation frequency  $\gamma/\pi\hbar$  sets the upper speed limit for quantum charge transport in this system in the absence of coherent driving, so half of the Rabi oscillation period sets the lower limit for physical electron transfer times:  $t_{ET} > \pi\hbar/2\gamma$ . Here, with  $P_D^{(thresh)} = 0.2$ ,  $t_{ET} = 37.5$  ps, which satisfies  $t_{ET} > \pi\hbar/2\gamma \simeq 1$  ps. The result for  $t_{ET}$  is plausible because  $t_{ET}$  does not violate its lower limit  $\pi\hbar/2\gamma$  and the result is well below the biological time scale of ms for actuating GPCRs [26].

#### *Calculation of Power Dissipation, $\bar{p}_{diss}$*

Power dissipation may be calculated within this model. This calculation is summarized here, but a full derivation of power dissipation is given in Appendix A. Power dissipation here is given by

$$p_{diss} = -p_{\mathcal{E},ev} - p_{\mathcal{E},v} - p_{\mathcal{E},e} , \quad (3.12)$$

where

$$\begin{aligned} p_{\mathcal{E},ev} &= \text{Tr} \left( \mathfrak{D} \hat{H}_{ev} \right) , \\ p_{\mathcal{E},v} &= \text{Tr} \left( \mathfrak{D} \hat{H}_v \right) , \text{ and} \\ p_{\mathcal{E},e} &= \text{Tr} \left( \mathfrak{D} \hat{H}_e \right) . \end{aligned} \quad (3.13)$$

We interpret  $p_{\mathcal{E},ev} + p_{\mathcal{E},v} + p_{\mathcal{E},e}$  as the rate of work done on the electron+odorant system by the environment.

Average power dissipation,  $\bar{p}_{diss}$ , is evaluated over the electron transfer time  $t_{ET}$ :

$$\bar{p}_{diss} = \frac{1}{t_{ET}} \int_0^{t_{ET}} p_{diss}(s) ds . \quad (3.14)$$

## CHAPTER FOUR

### Results

Results are presented in three different regimes: (A) in the limit of dominant indirect coupling (weak direct electron-environment coupling,  $\xi \rightarrow \infty$ ); (B) in the limit of dominant direct electron-environment coupling (weak indirect electron-phonon-environment coupling,  $\xi \rightarrow 0$ ); and (C) an intermediate regime, in which both couplings are present, but neither is dominant.

#### *Indirect Coupling Dominates*

When indirect coupling provides the dominant dissipation pathway, a rich set of spectroscopic behaviors is seen. Here, we explore the relationship between rate and odorant frequency, odorant reorganization energy, tunneling energy and temperature, and power dissipation.

#### *Resonant Peaks in ET Rate*

When indirect coupling is dominant ( $\xi \rightarrow \infty$ ), electron transfer rates exhibit resonant peaks. Figure 4.1 shows the ET rate  $k$  as a function of odorant vibrational angular frequency  $\omega_o = 2\pi f_o$ . The frequency axis is scaled in units of  $\Delta = E_D - E_A$ . Resonant peaks in  $k(f_o)$  occur at frequencies  $\omega_o = \Delta/s\hbar$ , where  $s$  is a positive integer. As odorant environmental coupling ( $\chi_v$ ) increases, the spectral peaks broaden.

The resonance of Figure 4.1 can be understood in the limit of  $\lambda = 0$ ,  $\gamma = 0$  and  $T = 0$ . Here, the eigenstates of the system are product states  $|X\rangle \otimes |n\rangle = |Xn\rangle$ , with eigenenergies  $E_X + \hbar\omega_o(n + 1)/2$  for occupation number  $n \in \{0, 1, 2, \dots\}$  and  $X \in \{D, A\}$ . This spectrum is depicted in Figure 4.2. The initial state is approximately  $|D0\rangle$ , with energy  $E_D + \hbar\omega_o/2$ . If  $\Delta = E_D - E_A = s\hbar\omega_o$  for some positive integer  $s$ , then the initial energy  $E_D + \hbar\omega_o/2$  matches exactly the eigenenergy

$E_A + \hbar\omega_o(s + 1)/2$ , facilitating an  $D \rightarrow A$  electron transfer event from the combined state  $|D0\rangle$  to  $|As\rangle$ . In order for the system to settle to  $|A0\rangle$  and for the electron transfer to “complete” ( $P_D \rightarrow 0$ ), the energy  $s\hbar\omega_o$  must be dissipated. Thus, low  $s$  minimizes the vibrational energy dissipation and time required for the ET event, and peaks in the rate  $k$  grow larger with decreasing  $s$ , with  $s = 1$  providing the highest peak. Multi-phonon processes—infrequently-considered in the theory of olfactory IETS—could play a role. In this model, ET rates are increased when the energy of fewer phonons must be dissipated to allow the system to settle to  $|A0\rangle$ .

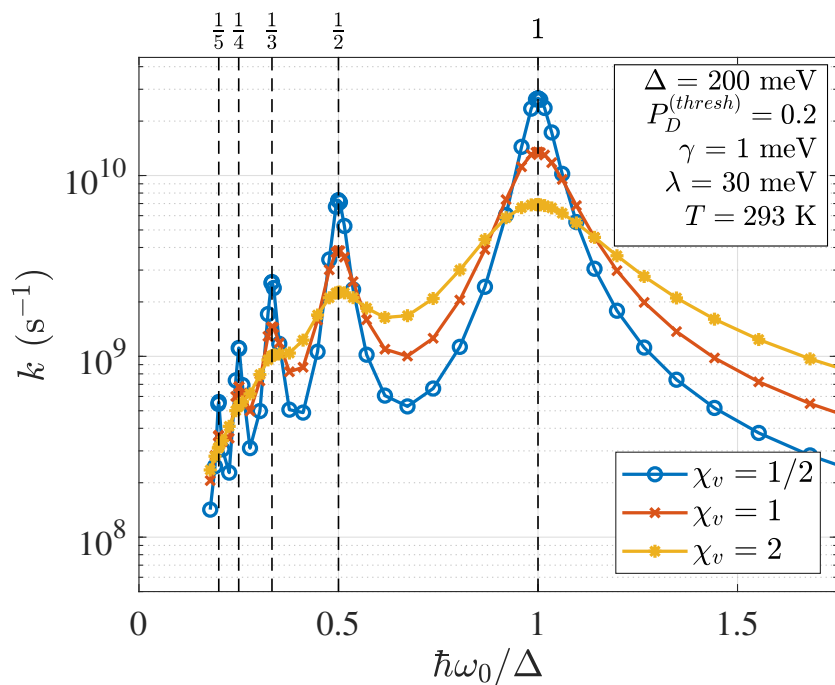


Figure 4.1: The electron transfer rate,  $k$ , from state  $|D\rangle$  to state  $|A\rangle$  exhibits resonant tunneling and environmentally-driven broadening of peaks. Here, peaks occur under a resonant condition that arises when the detuning  $\Delta = E_D - E_A$  is equal to an integer multiple of the vibrational quantization  $\hbar\omega_o$ . Additionally, resonant peaks are broadened as odorant-environment coupling increases, as quantified by  $\chi_v$ .

#### *Odorant Reorganization Energy, $\lambda$*

The absence of the odorant is modeled in the limit of  $\lambda \rightarrow 0$ . Since coupling between the ET event and the environment already is negligible, the electronic system

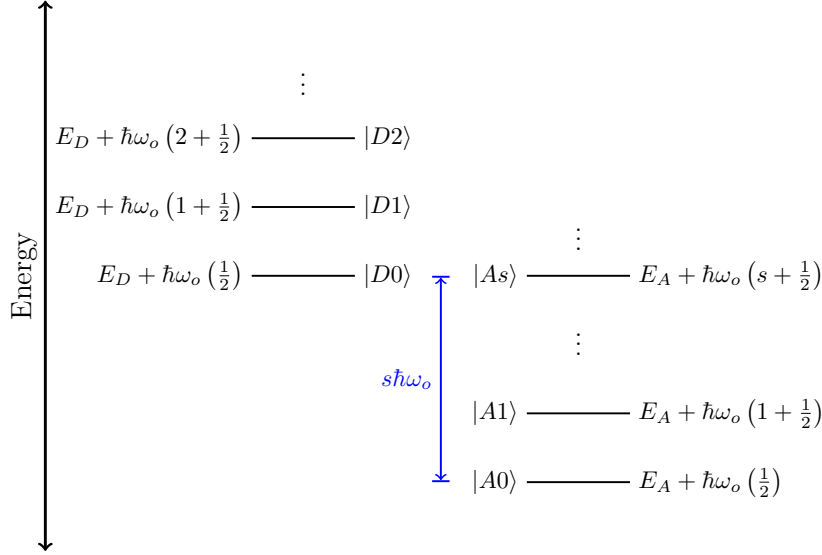
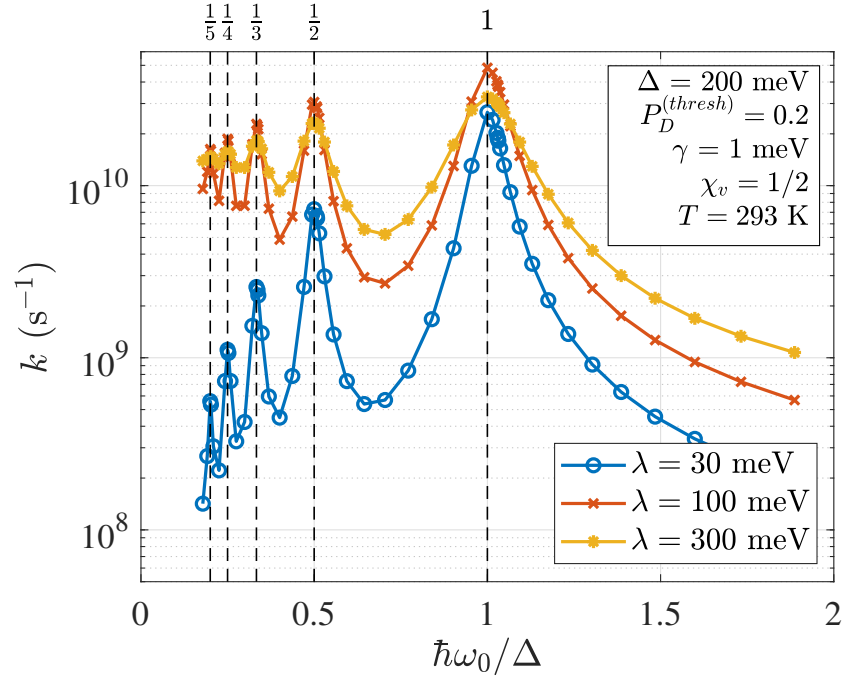


Figure 4.2: The eigenenergy spectrum for the system results in a resonant effect for the ET rate  $k$ . In the limit of  $\gamma = \lambda = T = 0$ , the eigenstates are  $|Xn\rangle$ , with energies  $E_X + \hbar\omega(n + 1/2)$ . When  $\Delta = E_D - E_A = s\hbar\omega$  for some integer  $s$ , a resonant transition  $|D0\rangle \rightarrow |As\rangle$  is favorable, as is the resonant back-transition  $|As\rangle \rightarrow |D0\rangle$ . The probability  $P_D$  does not decrease to a small value until the system can dissipate energy for the state to approach  $|A0\rangle$ . Since this dissipation takes time, the minimum non-zero value ( $n = 1$ ) enables the fastest dissipation and thus the fastest ET time and the highest ET rate  $k$ .

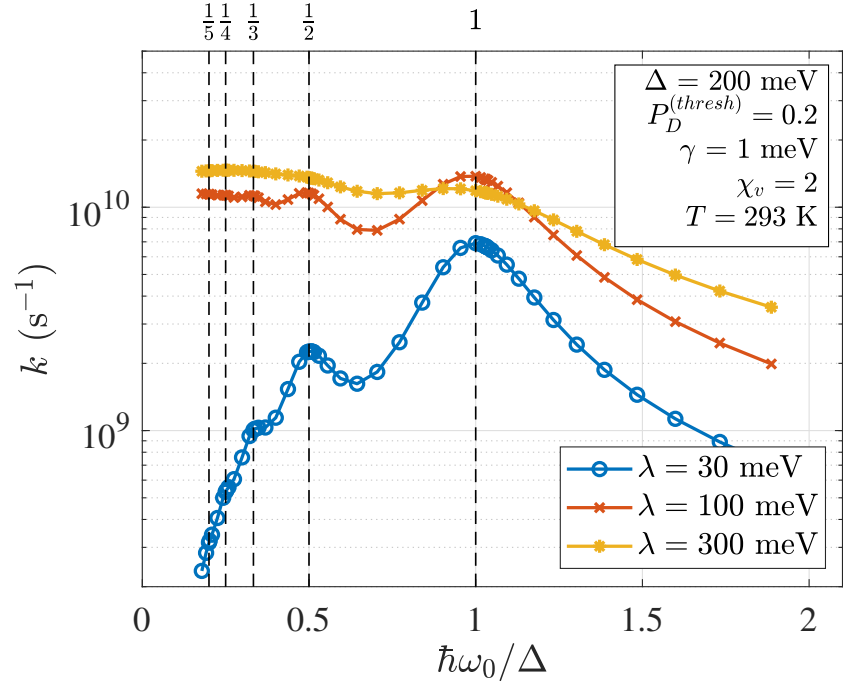
is unable to dissipate energy. Thus, the  $|D\rangle \rightarrow |A\rangle$  transition becomes less likely because of the non-negligible detuning  $\Delta$ , and rate decreases to zero. This is seen in Figure 4.3. On the other hand, increasing  $\lambda$  strengthens the electron-vibration coupling. An excessively strong coupling (high  $\lambda$ ) broadens the peaks in  $k(\hbar\omega_o/\Delta)$ . Figure 4.3 shows that increasing the reorganization energy  $\lambda$  contributes to a higher electron transfer rate  $k$  for lower frequencies. Resonant peaks are broadened as  $\lambda$  increases. The  $\lambda$ -dependence of rate  $k$  seen here appears to be consistent with Fermi's golden rule.

#### *Tunneling Energy, $\gamma$*

The results of Figure 4.4 shows that increasing the tunneling energy  $\gamma$  enables a higher electron transfer rate. This is consistent with the fact that the upper speed

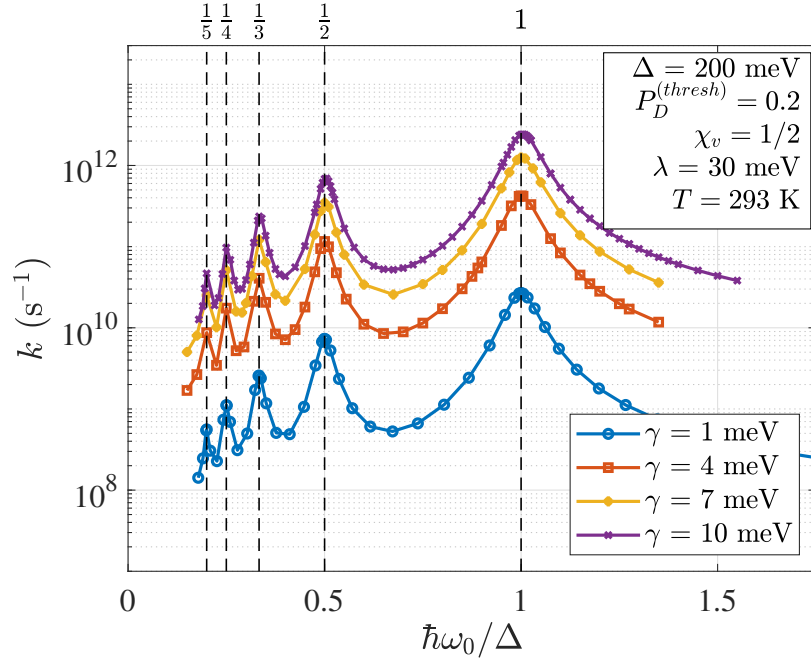


(a)  $\chi_v = 1/2$

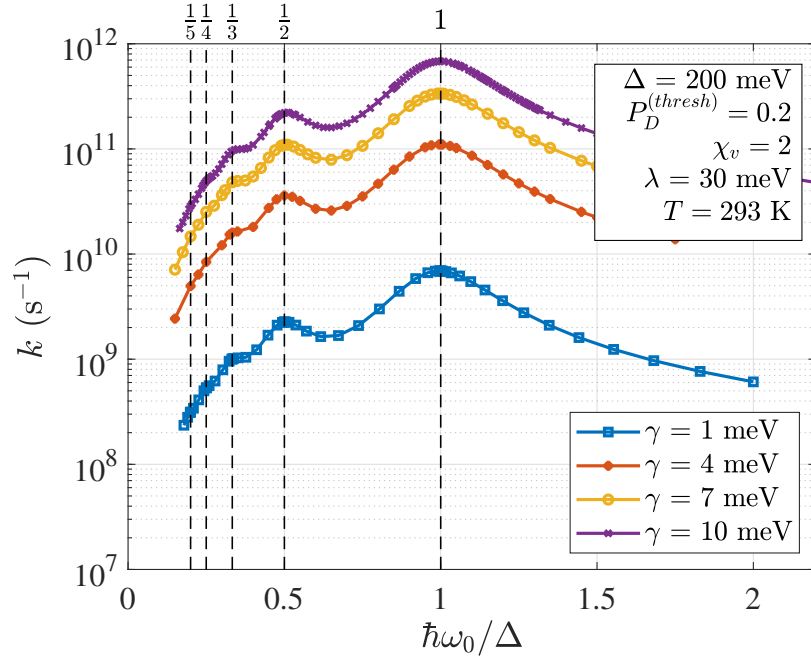


(b)  $\chi_v = 2$

Figure 4.3: Resonant peaks in  $k(f_o)$  are broadened as odorant reorganization energy,  $\lambda$ , is increased. Also, increasing  $\lambda$  contributes to a higher ET rate,  $k$ , for lower frequencies. This is seen in subfigure (a) for a weaker odorant-environment coupling,  $\chi_v = 1/2$ , and again in subfigure (b) for a stronger coupling,  $\chi_v = 2$ .



(a)  $\chi_v = 1/2$



(b)  $\chi_v = 2$

Figure 4.4: Increase in tunneling energy,  $\gamma$ , contributes to higher electron transfer rate,  $k$ , from state  $|D\rangle$  to state  $|A\rangle$ . This is shown for weak odorant-environment coupling,  $\chi_v = 1/2$  in subfigure (a) and for strong odorant-environment coupling,  $\chi_v = 2$  in subfigure (b).

limit of electron transfer is the Rabi oscillation frequency  $\pi\gamma/\hbar$ . Additionally, the  $\gamma$ -dependence of rate  $k$  seen here appears to be consistent with Fermi's golden rule.

### Temperature, $T$

Figure 4.5 shows ET rate  $k$  as a function of temperature,  $T$ . In the zero-temperature limit, a non-zero  $k$  reveals the quantum nature of the system, as a classical or semi-classical prediction for the ET rate would be zero in the absence of thermal excitation. For terrestrial and biological temperatures  $T < 300$  K, ET rate  $k$  is largely constant. As  $T$  increases to high temperatures ( $k_B T \sim \hbar\omega_o$ ),  $k$  begins to

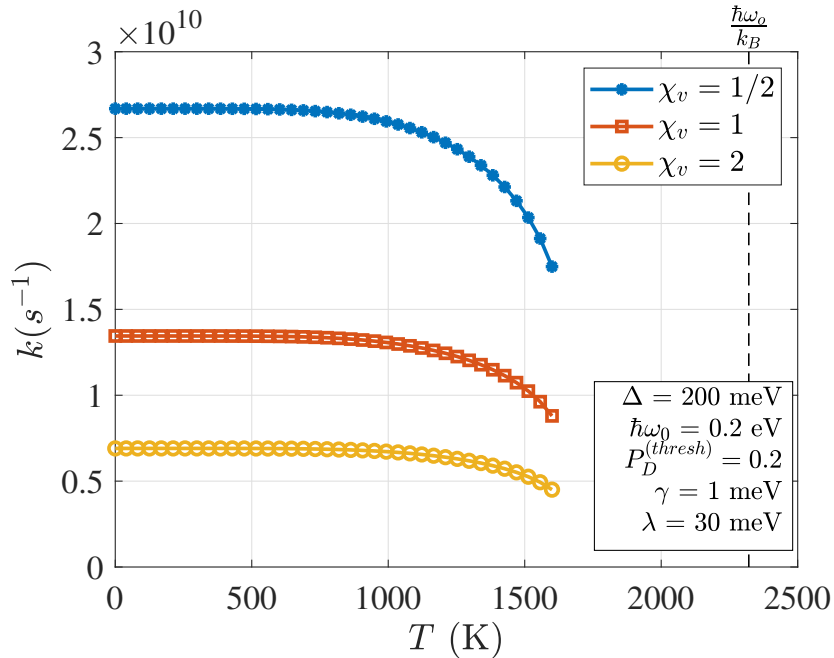


Figure 4.5: Electron transfer rate,  $k$ , from state  $|D\rangle$  to state  $|A\rangle$  is largely temperature-independent at terrestrial temperatures and below. ET rate is shown here as a function of environmental temperature  $T$  for different values of odorant-environment coupling  $\chi_v$ . When  $T$  is sufficiently large that  $k_B T \sim \hbar\omega$ , ET rate decreases since thermal environmental fluctuations enable  $|A\rangle \rightarrow |D\rangle$  excitation.

decrease. This is because as  $T$  increases, the system is increasingly thermally excited, raising the probability  $P_D(t)$  of finding the electron on the  $D$  site. This increases the time  $t_{ET}$  it takes for  $P_D(t)$  to decay to the threshold defined in our calculation, thus

decreasing  $k$ . While the temperature-dependence of  $k$  from this model is largely consistent with Fermi's golden rule, a point of divergence between the two models is rate behavior at low temperature. Fermi's golden rule predicts  $k = 0$  at  $T = 0$ ; however, the present model predicts  $k \neq 0$  at  $T = 0$ .

Interestingly, a quantum-to-classical transition emerges when we consider how temperature  $T$  and oscillator frequency  $\omega_o$  affect rate  $k$ . Figure 4.6 shows calculations of  $k$  for various values of  $\omega_o$  and  $T$ . For low  $\omega_o$ , reducing  $T$  decreases the ET rate  $k$ . This result is consistent with classical and semi-classical rate models, which require thermal excitation to cross a potential barrier.

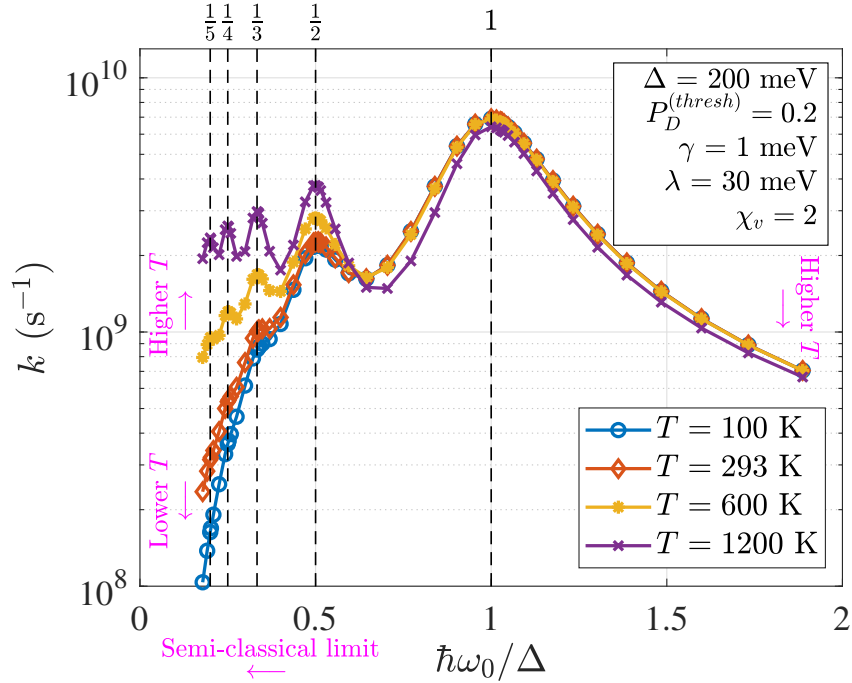


Figure 4.6: Model ET rates exhibit both quantum and classical/semi-classical behaviors over the spectrum of odorant frequencies  $f_o$ . In the low frequency limit ( $\hbar\omega_o \ll \Delta$ ), increasing temperature increases the rate  $k$  in a behavior consistent with a classical or semi-classical system in which thermal excitation allows the system to surmount a classical barrier. In the high-frequency limit ( $\hbar\omega_o \gg \Delta$ ), ET rate,  $k$ , decreases with a significant increase in temperature. This is consistent with the behavior noted in Section 4.

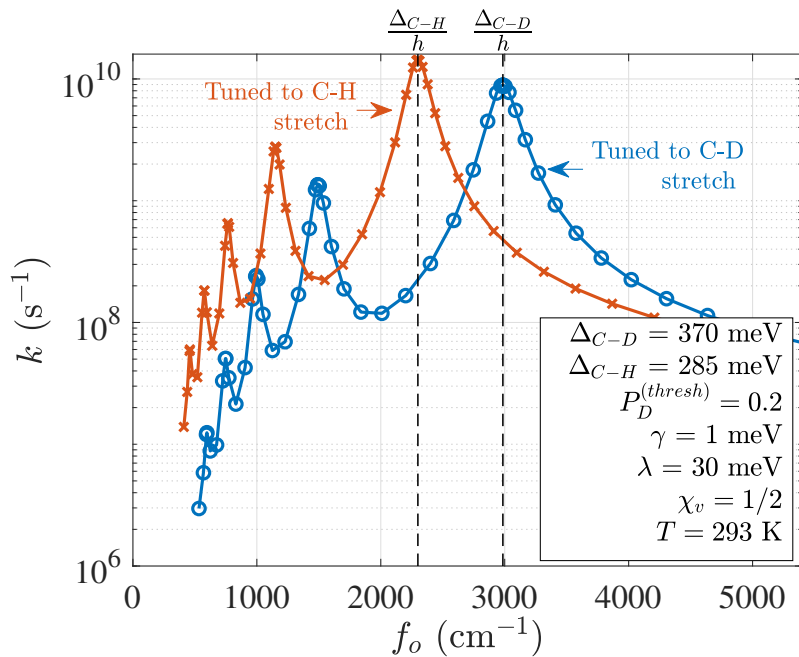
For low  $\omega_o$ , the fully-quantum system gives rise to this semi-classical behavior because lowering  $\omega_o$  reduces the spacing between eigenvalues of the fully-quantum

system (see Figure 3.2). For low-enough  $\omega_o$ , the energy quantization in the fully-quantum model is small compared to the barrier height between states  $|D\rangle$  and  $|A\rangle$  in the semi-classical system. Thus, the semi-classical behaviors of the system will be dominant. On the other hand, when  $\omega_o$  is large, energy quantization in the system is significant, the system manifests more quantum mechanical behaviors. Here, increasing  $T$  only slightly decreases  $k$ , as discussed previously. With large  $\omega_o$ , a high rate  $k$  persists, even at low temperature,  $T = 0$ . This is a truly non-classical result.

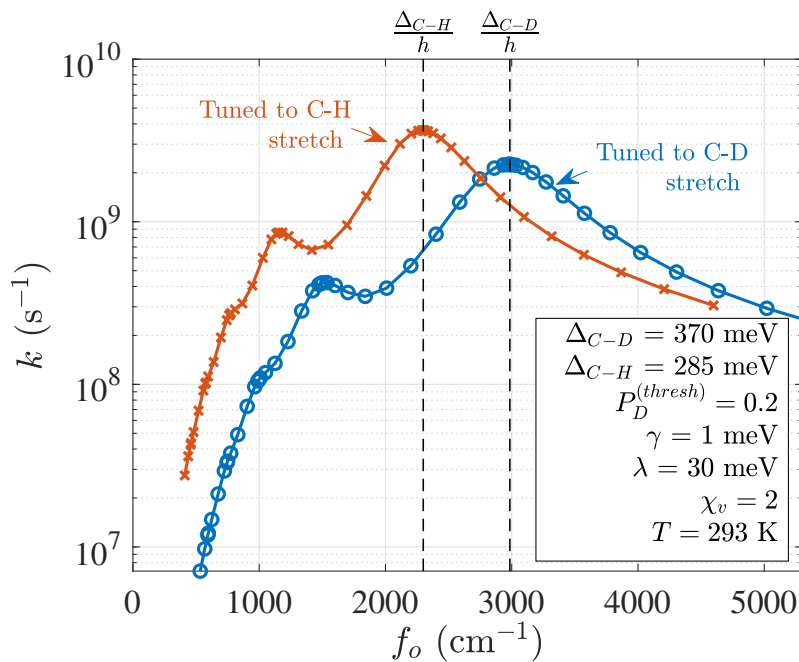
### *Discrimination between Isotopomers*

Next, the model developed here is applied to the study of receptor selectivity in the odorant-receptor complex response to isotopomers. Specifically, we considered a receptor's ability to spectroscopically distinguish acetophenone from its fully-deuterated isotopomer acetophenone-d8. Here, we assume that the C-H and C-D stretch play the distinguishing role [5, 12].

Figure 4.7 shows the spectroscopic response of  $k$  for two receptors: one receptor is resonantly tuned to the C-H stretch frequency  $f_o^{(C-H)} = 2300 \text{ cm}^{-1}$  by setting  $\Delta = \Delta_{C-H} = \hbar\omega_o^{(C-H)}$ , and another is resonantly tuned to the C-D stretch frequency  $f_o^{(C-D)} = 3000 \text{ cm}^{-1}$  by setting  $\Delta = \Delta_{C-D} = \hbar\omega_o^{(C-D)}$ . The response of each receptor is calculated for various values of  $\omega_o$ , and the strongest resonant peak occurs as expected for the preferred odorant when  $\Delta = \hbar\omega_o$ . For each receptor, if odorant-environment coupling is weak ( $\chi_v = 1/2$ ), the ET rate  $k$  drops by almost two orders of magnitude when the non-preferred isotopomer is in the receptor. For a stronger odorant-environment coupling ( $\chi_v = 2$ ), spectral broadening results in the spectroscopic  $k(\omega_o)$  response, and rate drops by more than 50% when the preferred molecule is replaced by its isotopomer. Increased environmental coupling reduces the receptor's selectivity to its preferred odorant.



(a)  $\chi_v = 1/2$



(b)  $\chi_v = 2$

Figure 4.7: The model developed here exhibits a differential response to isotopomers. (a) A receptor tuned to the C-H stretch responds to the C-H stretch with a rate  $k$  that is more than one order of magnitude higher than the rate due to the presence of a C-D stretch vibrational mode. A receptor tuned to the C-D stretch exhibits a similarly higher ET rate when an odorant with a C-D ligand is present than when an odorant with a C-H ligand is present. (b) Peak broadening occurs with stronger odorant-environmental coupling, and the change in rate between isotopomers is reduced for each receptor.

### Power Dissipation

The dissipation of power and energy is essential to a  $|D\rangle \rightarrow |A\rangle$  transition. A plot of average power dissipation  $\bar{p}_{\text{diss}}$  (see Figure 4.8) for various odorant frequencies shows that the system dissipates the highest rates of average power at frequencies satisfying  $\Delta = s\hbar\omega_o$  for some positive integer  $s$ . This coincides exactly with the resonant peaks in rate (see Figure 4.1), underscoring the enabling role dissipation plays in this process: the more quickly the electron can dissipate power, the faster it can make the  $|D\rangle \rightarrow |A\rangle$  transition, increasing the ET rate. This relationship is a direct consequence of the conservation of energy, and the ET is thus facilitated by its ability to relax by  $\Delta$  via the excitation of odorant phonons or by dissipating power to the thermal environment.

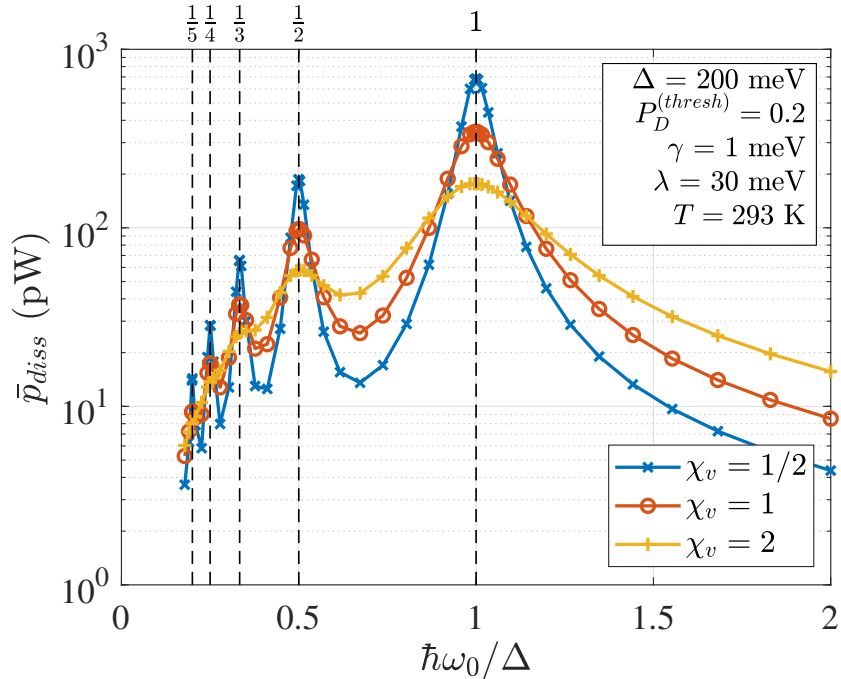


Figure 4.8: Power dissipation  $\bar{p}_{\text{diss}}$  to the environment exhibits a frequency-dependence very similar to the the frequency dependence of rate  $k$  to odorant frequency (compare with Figure 4.1). Peaks for  $\bar{p}_{\text{diss}}$  occur when  $\Delta = s\hbar\omega_o$  for some integer  $s$ , and resonant peaks broaden with stronger odorant-environment interaction (increasing  $\chi_v$ ).

The relationship between rate  $k$  and  $\bar{p}_{\text{diss}}$  exhibits a highly linear relationship, as seen in the scatter plot of Figure 4.9. This scatter plot shows the correlation between the rate data from Figure 4.1 and the power dissipation data of Figure 4.8. One regression line is remarkably effective for three different odorant-environment coupling strengths ( $\chi_v \in \{0.5, 1, 2\}$ ).

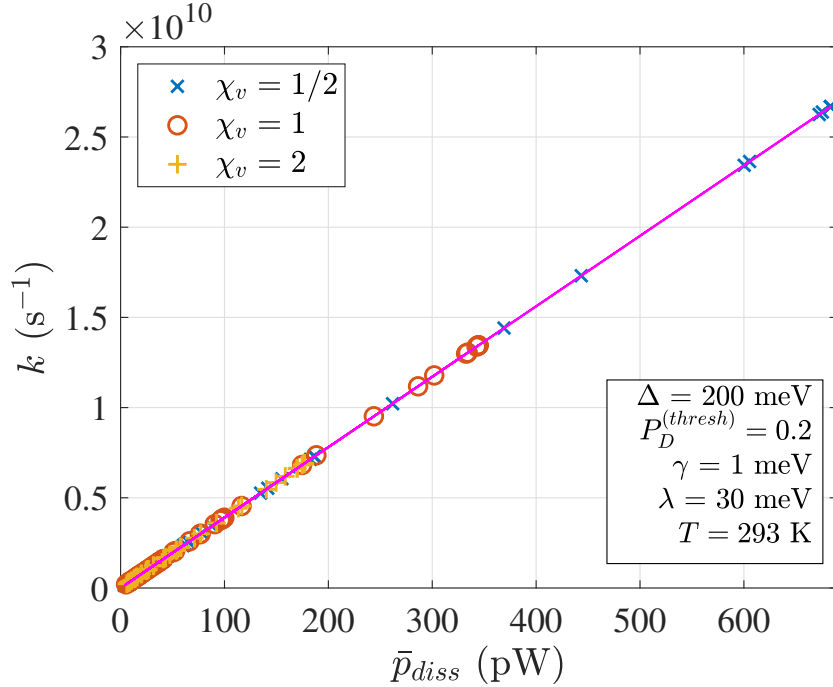
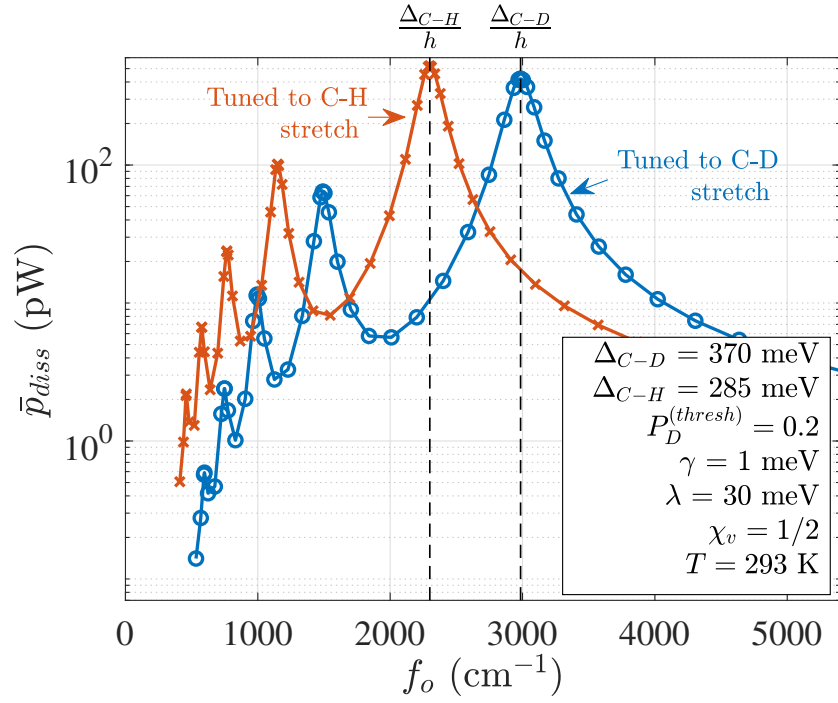


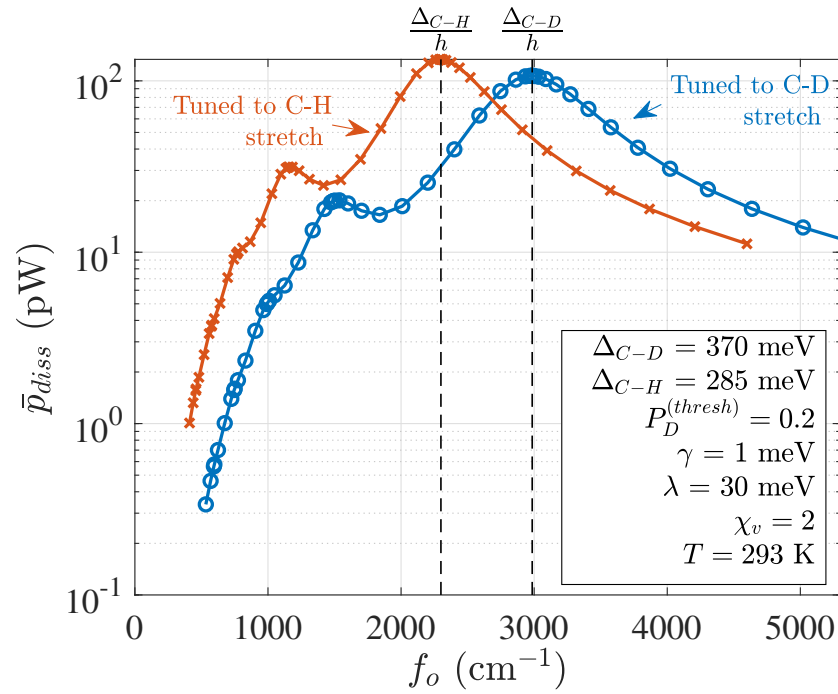
Figure 4.9: Power dissipation  $\bar{p}_{\text{diss}}$  exhibits a linear correlation with ET rate. This scatter plot of rate data from Figure 4.1 and power dissipation data from Figure 4.8 shows a highly linear relationship between the two sets of data. A fitting line is drawn in purple, and the data lies along this same line for several odorant-environment coupling strengths.

Finally, we use power dissipation to quantify the selectivity of a receptor within this model to its preferred isotopomer. Power dissipation  $\bar{p}_{\text{diss}}$  is plotted as a function of odorant frequency  $f_o$  in Figure 4.10. The power dissipation curves of Figure 4.10 are very similar to the rate-versus-frequency curves for the same receptors (see Figure 4.7).

We quantify receptor selectivity by taking the ratio of power dissipation at the characteristic vibrational frequency of the preferred odorant to the rate of power dis-



(a)  $\chi_v = 1/2$



(b)  $\chi_v = 2$

Figure 4.10: Average power dissipation to the environment is frequency-selective—and therefore ligand-selective. Power dissipation peaks when a receptor tuned to the C-H (or C-D) stretch couples to a ligand with a frequency  $f_o$  matching the frequency of the C-H (or C-D) stretch. This is shown for weak odorant-environment coupling,  $\chi_v = 1/2$  in subfigure (a) and for strong odorant-environment coupling,  $\chi_v = 2$  in subfigure (b).

sipation at the frequency characteristic of the non-preferred odorant. For the receptor tuned to the C-H (or C-D) stretch mode, we use power dissipation in the presence of a C-H (or C-D) bond and divide by the power dissipation in the presence of a C-D (or C-H) stretching mode. With an odorant-environment coupling of  $\chi_v = 1/2$ , selectivity for the preferred odorant is  $\sim 15$  dB (see Table 4.1). Stronger odorant-environment coupling ( $\chi_v = 2$ ) broadens the peaks in the  $\bar{p}_{\text{diss}}(f_o)$  curve, and selectivity drops to  $\sim 5$  dB (see Table 4.2).

Table 4.1: Power dissipation from the receptor-odorant complex to the environment is enhanced when a ligand is present for which the receptor is tuned (i.e.,  $\Delta = \hbar\omega_o$ ). When the preferred ligand is replaced by its relative isotopomer, then,  $\Delta \neq \hbar\omega_o$ , and power dissipation is suppressed by  $\sim 15.4$  dB. This frequency-selective dissipation is used to quantify the selectivity of the receptor to a particular vibrational mode. Here, indirect coupling,  $\chi_v = 1/2$ .

Receptor tuned to	Power dissipation (pW)		Selectivity (dB)
	C-H Stretch	C-D Stretch	
C-H stretch	521.7	17.2	14.81
C-D stretch	10.6	420.7	16

Table 4.2: In analogy to Table 4.1, receptor selectivity is calculated and tabulated for stronger odorant-environment coupling ( $\chi_v = 2$ ). Increased odorant-environment coupling broadens the resonant peaks in power, reducing receptor selectivity to  $\sim 5$  dB (compare to Table 4.1).

Receptor tuned to	Power dissipation (pW)		Selectivity (dB)
	C-H Stretch	C-D Stretch	
C-H stretch	133.4	46.1	4.62
C-D stretch	31.4	106.9	5.32

### *Direct (Electron-environment) Coupling Dominates*

When direct electron-environment coupling provides the strongly-dominant dissipation path ( $\xi \rightarrow 0$ ), spectroscopic behaviors vanish, and rate becomes largely independent of the vibrational frequency of the odorant. This is seen in Figure 4.11. Here, a raised electron-environment coupling (increasing  $\chi_e$ ) enables a faster relaxation and a higher ET rate  $k$ .

A very subtle resonant effect in rate is seen if  $\chi_e$  is low. Slight deviations in the ET rate at resonant frequencies ( $\omega_o = s\Delta/\hbar$  for some integer  $s > 0$ ) are revealed (see data for  $\chi_e = 0.01$ ). These deviations are due to a transient response in which a resonant condition arises, and the conservation of energy facilitates rapid power transfer from electron to an integer number of odorant phonons. This allows a faster ET: the probability  $P_D(t)$  crosses the threshold  $P_D^{(thresh)}$  sooner, resulting in a slightly higher rate  $k$ . However, since this energy cannot be dissipated from the odorant to the environment, the energy is subsequently transferred back to the electron, with some  $|A\rangle \rightarrow |D\rangle$  back-transfer, and a  $P_D(t)$  that had crossed below  $P_D^{(thresh)}$  may cross above  $P_D^{(thresh)}$  again.

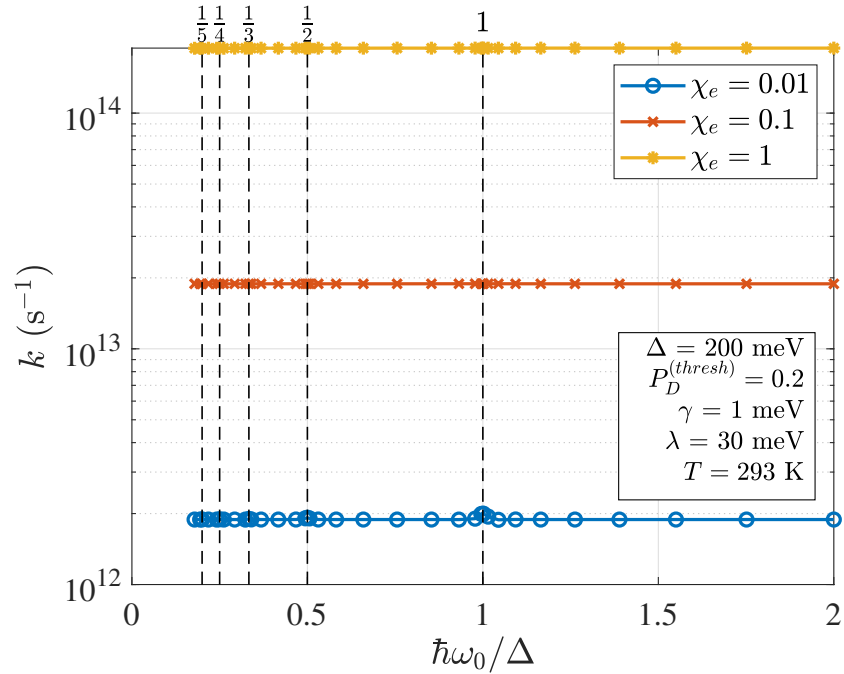


Figure 4.11: Resonant behaviors are almost completely suppressed when the indirect dissipation path is disrupted by severing the odorant-environment connection ( $\chi_v \rightarrow 0$ ). Here, the rate is largely independent of odorant vibrational frequency  $f_0$  and is determined solely by the strength of direct dissipation  $\chi_e$ . ET rate increases with increasing direct electron-environment coupling  $\chi_e$ .

Figure 4.12 shows that the direct electron-to-environment interaction indeed drives an exponential relaxation characterized by time constant  $T_e$ . Here,  $E(t) = \text{Tr} \left( \hat{H} \hat{\rho}(t) \right)$ , the expectation value of energy, is plotted with an exponential fit, given by

$$f_E(t) = E(\infty) + (E(0) - E(\infty)) (1 - e^{-t/T_e}) . \quad (4.1)$$

The calculated  $E(t)$  from the model matches the exponential  $f_E(t)$  very precisely.

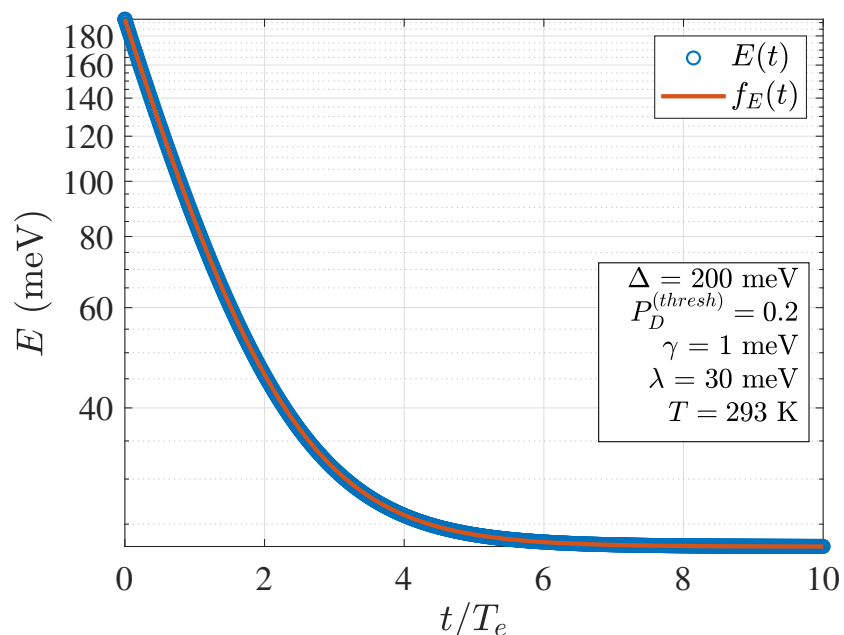


Figure 4.12: The direct electron-environment dissipation path drives an exponential relaxation with time constant  $T_e$ . Here,  $T_e = 33$  fs, and electron+odorant total energy  $E(t)$  matches an exponential fit  $f_E(t)$ .

### *Both Direct and Indirect Coupling are Significant*

Here, we explore the case in which neither the direct nor indirect dissipative pathways are negligible. In Figure 4.13, the resonant peaks in the rate  $k$  become less pronounced as the system transitions from an indirect-coupling-dominated (larger  $\xi$ ) to direct-coupling-dominated (smaller  $\xi$ ). This is because the additional (direct) dissipative pathway assists the electron transfer, raising the ET rate most noticeably in the non-resonant regions ( $\Delta \neq s\hbar\omega_0$  for positive integers  $s$ ) where ET was most

highly suppressed with high  $\xi$  (compare Figure 4.1 to the red and blue traces of Figure 4.13). If  $\xi$  becomes small enough, the spectroscopic response of  $k(f_0)$  vanishes as the direct dissipative pathway dominates and the resonant behavior of the indirect dissipation path is masked.

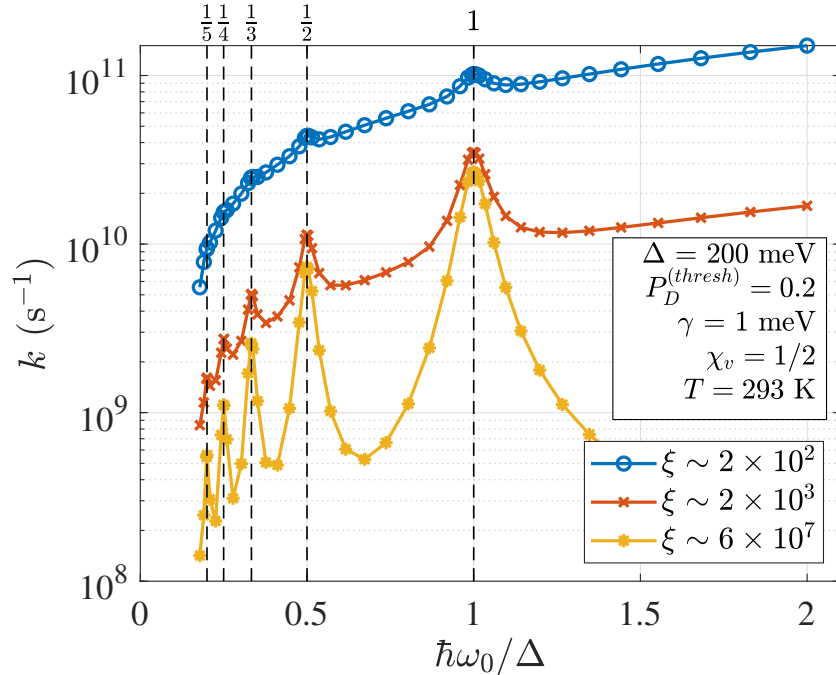
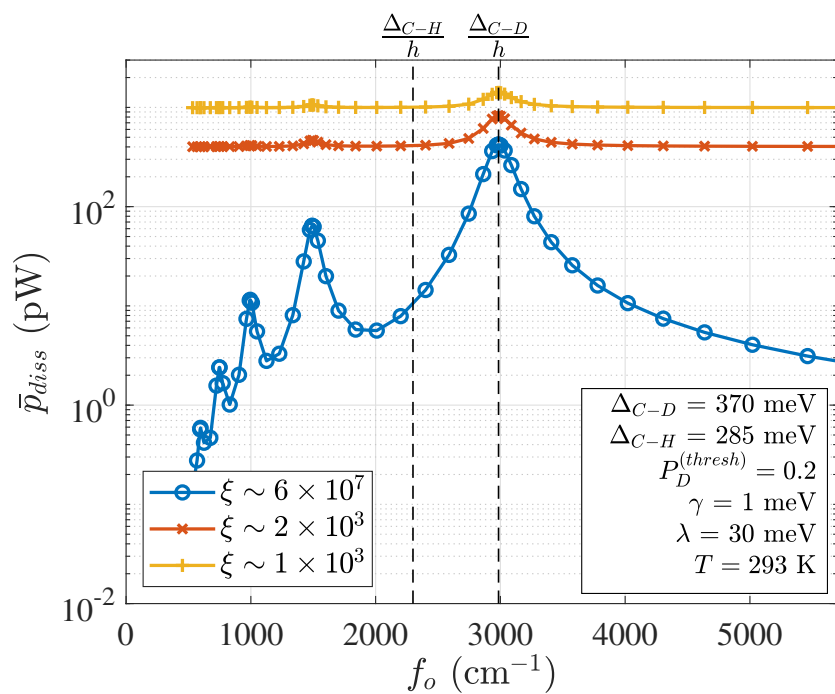


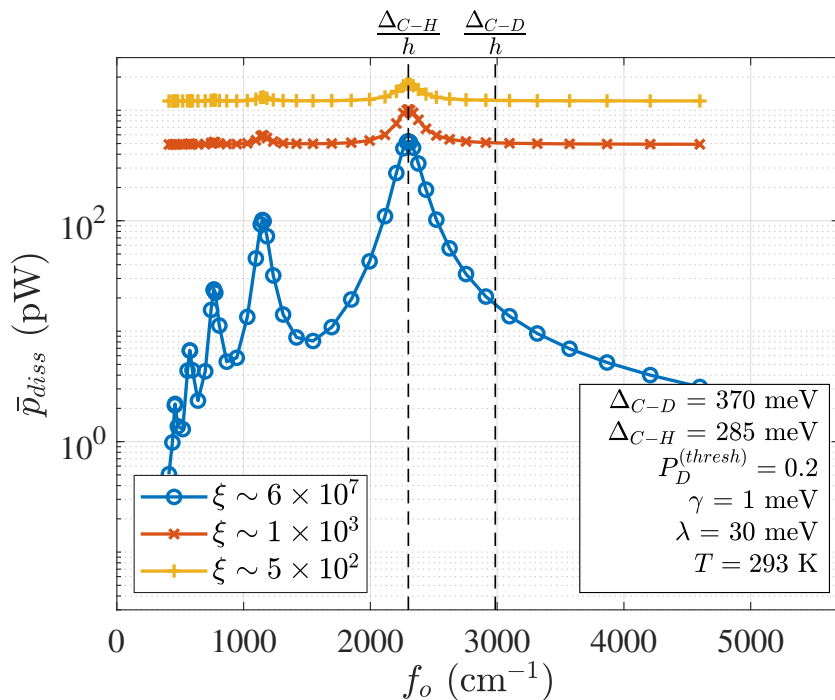
Figure 4.13: As the strength of direct coupling is increased ( $\xi$  decreases), the resonant peaks broaden, and spectroscopic behaviors in the ET rate become masked.

The degradation of the receptor spectroscopy is also seen in the dissipation plots of Figure 4.14. For high  $\xi$ , the spectroscopic behaviors are readily seen in strong peaks in the dissipation curve  $\bar{p}_{\text{diss}}(f_o)$ . As  $\xi$  is reduced, spectroscopic behaviors are less pronounced as direct-path dissipation begins to compete with the indirect-path dissipation, enabling higher levels of dissipation in previously-suppressed (non-resonant) frequencies. Eventually, the spectroscopic behavior is completely masked as  $\xi$  is further reduced.

The loss of spectroscopic behaviors with reduced  $\xi$  can be quantified in the selectivities of the receptors tuned to either the C-D or C-H stretch modes. Selectivity



(a) Receptor tuned to C-D



(b) Receptor tuned to C-H

Figure 4.14: Spectroscopic effects in power dissipation are masked with increasing direct-path dissipation (decreasing  $\xi$ ) for receptors tuned to a specific isotopomer. Subfigure (a) is for a receptor tuned to the C-D stretch frequency, and (b) is for a receptor tuned to the C-H stretch frequency.

for these receptors is listed in Tables 4.3 and 4.4 for the case where  $\chi_v = 1/2$ . High values of  $\xi$  yield the receptor selectivities seen in the indirect-path-dominant regime (see Table 4.1). When  $\xi$  is reduced enough, selectivity is degraded so that isotopomers are no longer distinguishable (selectivity is below  $\sim 3$  dB).

Table 4.3: Strengthening the direct electron-environment dissipation path (i.e., decreasing  $\xi$ ) degrades the sensitivity of a receptor tuned to the C-D stretch frequency. Here,  $\chi_v = 1/2$ .

Receptor tuned to C-D stretch	
Indirect to direct coupling ratio, $\xi$	Selectivity (dB)
$6 \times 10^7$	16.0
$2 \times 10^3$	3.0
$1 \times 10^3$	1.5

Table 4.4: Strengthening the direct electron-environment dissipation path (i.e., decreasing  $\xi$ ) degrades the sensitivity of a receptor tuned to the C-H stretch frequency. Here,  $\chi_v = 1/2$ .

Receptor tuned to C-H stretch	
Indirect to direct coupling ratio, $\xi$	Selectivity (dB)
$6 \times 10^7$	14.8
$1 \times 10^3$	3.0
$5 \times 10^2$	1.5

## CHAPTER FIVE

### Conclusion

A numerical model was presented for olfactory IETS in which the two-state electronic system was coupled to a thermal environment in two ways: (1) directly, and (2) indirectly via a quantum harmonic oscillator modeling the environmentally-damped dominant vibrational mode of the odorant molecule. This model treats explicitly a dominant odorant vibrational mode and provides a method for calculating dissipation from the electron to the environment via both pathways. Resonances were observed in the ET rate for odorant frequencies  $\omega_o = \Delta/s\hbar$  when indirect electron-environment coupling is dominant, consistent with the vibrational theory of olfaction. The resonance in the ET process is related to the system's ability to dissipate energy to the environment via the indirect pathway only. In this limit, the model also demonstrates a transition between semi-classical and quantum behavior based on the size of the quantization  $\hbar\omega_o$ . Odorants with small vibrational quantization  $\hbar\omega_o$  exhibit an ET rate behavior in which decreasing temperature reduces the ET rate, consistent with classical and semi-classical ET rate models where thermal excitation provides the means to pass over a potential energy barrier. On the other hand, when  $\hbar\omega_o \sim \Delta$ , odorant quantization becomes significant, and reducing the temperature of the reservoir has less effect on ET rate because quantum mechanical tunneling becomes a more dominant effect. Also, this model predicts significant ET rates even at  $T = 0$  K, contrary to Fermi's golden rule. Behavior like this is unique to quantum mechanical models. Spectroscopic behaviors in the ET rate become masked as direct electron-environment coupling plays a stronger role in the ET. Nonetheless, the spectroscopic behaviors may be relevant in some biological systems for which the direct dissipative path is negligible.

The vibrational theory of olfaction is an interesting application of quantum mechanics that requires further experimental techniques and developments for validation. Experimental work will be required to validate this and other models of IETS, and even the vibrational theory of olfaction itself. No experiment has conclusively demonstrated a spectroscopic olfactory mechanism, nor identified the existence of the *D* and *A* sites, nor eliminated perireceptor events in distinguishing isotopomers. Further developments in the model could incorporate the inclusion of additional odorant vibrational modes, as well as a treatment of chirality in enantiomers.

Models like this may be used in exploring spectroscopic effects in GPCRs more broadly in mammalian nervous systems beyond olfactory receptors [27]. This may enable improved drug designs, as well as better drug dosage and effectiveness models, impacting the sciences of health and human performance. The results of this model may be relevant for the development of novel or improved artificial noses [28], with applications in security and anti-terrorism, and possibly the detection of some forms of cancer [29]. The treatment of vibrational theory of olfaction within this model may illuminate insect olfaction, yielding improved insect repellants, which can reduce the spread of vector-borne diseases.

## APPENDIX

## APPENDIX A

### Derivation of Power Expressions

#### *Power Flow in a Closed System*

Before deriving the expressions of (3.12)-(3.13) it is helpful to consider power transfer within the subcomponents of a simpler, closed system.

Let a closed system  $AB$  with Hamiltonian  $\hat{H}$  be partitioned so that there are two subsystems, labeled  $A$  and  $B$ , each described by its own respective Hamiltonian,  $\hat{H}_A$  or  $\hat{H}_B$ . For simplicity, it is assumed that the interaction between  $A$  and  $B$  is *included* within  $\hat{H}_B$  (this choice is arbitrary: the interaction may as well have been included in  $\hat{H}_A$ ). Thus,

$$\hat{H} = \hat{H}_A + \hat{H}_B . \tag{A.1}$$

The dynamics of the closed system's density matrix  $\hat{\rho}$  are given by the quantum Liouville equation:

$$\dot{\hat{\rho}} \equiv \frac{d\hat{\rho}}{dt} = -\frac{i}{\hbar} [\hat{H}, \hat{\rho}] . \tag{A.2}$$

Here we have introduced the more compact “dot” notation for a time derivative:  $\dot{\alpha} \equiv d\alpha/dt$ . The energy  $E_A$  for subsystem  $A$  is the expectation value of the Hamiltonian  $\hat{H}_A$ :

$$E_A \equiv \langle \hat{H}_A \rangle = \text{Tr} \left( \hat{H}_A \hat{\rho} \right) . \tag{A.3}$$

We obtain a power expression for subsystem  $A$  by differentiating (A.3).

$$p_A = \frac{d}{dt} E_A = \frac{d}{dt} \left( \text{Tr} \left( \hat{H}_A \hat{\rho} \right) \right) . \tag{A.4}$$

This power is to be interpreted as work done on subsystem  $A$ , or equivalently, power flux into subsystem  $A$ , since  $p_A > 0$  will raise  $E_A$ . The order of the trace and the time

differentiation both may be interchanged, yielding

$$p_A = \text{Tr} \left( \dot{\hat{H}}_A \hat{\rho} \right) + \text{Tr} \left( \hat{H}_A \dot{\hat{\rho}} \right) . \quad (\text{A.5})$$

If  $\hat{H}_A$  is constant (i.e.,  $\dot{\hat{H}}_A = 0$ ), then we can use (A.2) to eliminate  $\dot{\hat{\rho}}$  from (A.5):

$$p_A = -\frac{i}{\hbar} \text{Tr} \left( \hat{H}_A \left[ \hat{H}, \hat{\rho} \right] \right) . \quad (\text{A.6})$$

Using (A.1), the linearity of the trace, and the cyclic permutability of the trace, (A.6) becomes

$$p_A = -\frac{i}{\hbar} \text{Tr} \left( \left[ \hat{H}_A, \hat{\rho} \right] \hat{H}_A \right) - \frac{i}{\hbar} \text{Tr} \left( \left[ \hat{H}_B, \hat{\rho} \right] \hat{H}_A \right) . \quad (\text{A.7})$$

To analyze and interpret (A.7), it is helpful to examine an expression of the form of the second term, ignoring the  $-i/\hbar$  prefactor. It can be shown that  $\text{Tr} \left( \left[ \hat{X}, \hat{\rho} \right] \hat{Y} \right) = -\text{Tr} \left( \left[ \hat{Y}, \hat{\rho} \right] \hat{X} \right)$ :

$$\text{Tr} \left( \left[ \hat{X}, \hat{\rho} \right] \hat{Y} \right) = \text{Tr} \left( \hat{X} \hat{\rho} \hat{Y} \right) - \text{Tr} \left( \hat{\rho} \hat{X} \hat{Y} \right) \quad (\text{A.8})$$

$$= \text{Tr} \left( \hat{\rho} \hat{Y} \hat{X} \right) - \text{Tr} \left( \hat{Y} \hat{\rho} \hat{X} \right) \quad (\text{A.9})$$

$$= -\text{Tr} \left( \left[ \hat{Y}, \hat{\rho} \right] \hat{X} \right) . \quad (\text{A.10})$$

Here, (A.8) was obtained by the linearity of the trace, (A.9) by cyclically permuting each product in (A.8), and (A.10) by the linearity of the trace once again. One implication of (A.10) is that

$$\text{Tr} \left( \left[ \hat{X}, \hat{\rho} \right] \hat{Y} \right) = 0 \quad \text{when} \quad \hat{X} = \hat{Y} . \quad (\text{A.11})$$

Thus, the first term in (A.7) is identically zero, and the power input  $p_A$  to  $A$  reduces to

$$p_A = p_{B,A} \equiv -\frac{i}{\hbar} \text{Tr} \left( \left[ \hat{H}_B, \hat{\rho} \right] \hat{H}_A \right) . \quad (\text{A.12})$$

We recognize that in this closed system, power influx to  $A$  can come only from  $B$ , so (A.12) is interpreted as the power flowing from  $B$  to  $A$ , and we assign it the symbol  $p_{B,A}$ .

It also is shown here that when  $\hat{X}$  and  $\hat{Y}$  commute,  $\text{Tr} \left( [\hat{X}, \hat{\rho}] \hat{Y} \right) = 0$ :

$$\begin{aligned} \text{Tr} \left( [\hat{X}, \hat{\rho}] \hat{Y} \right) &= \text{Tr} \left( \hat{X} \hat{\rho} \hat{Y} \right) - \text{Tr} \left( \hat{\rho} \hat{X} \hat{Y} \right) \\ &= \text{Tr} \left( \hat{Y} \hat{X} \hat{\rho} \right) - \text{Tr} \left( \hat{X} \hat{Y} \hat{\rho} \right) \\ &= -\text{Tr} \left( [\hat{X}, \hat{Y}] \hat{\rho} \right) . \end{aligned}$$

Thus,

$$\text{Tr} \left( [\hat{X}, \hat{\rho}] \hat{Y} \right) = 0 \quad \text{when} \quad [\hat{X}, \hat{Y}] = 0 . \quad (\text{A.13})$$

### *Power Flow in an Open System*

The starting points for the power flow expressions of (3.12)-(3.14) are the energy equation

$$E = \langle \hat{H} \rangle = \text{Tr} \left( \hat{H} \hat{\rho} \right) , \quad (\text{A.14})$$

and the Lindblad equation

$$\dot{\hat{\rho}} = -\frac{i}{\hbar} [\hat{H}, \hat{\rho}] + \mathfrak{D} . \quad (\text{A.15})$$

In (A.14) and (A.15),  $\hat{H}$  is the Hamiltonian for the system, and  $\hat{\rho}$  is its density matrix. Equation (A.15) describes the dynamics of the system as an open system, with dissipator  $\mathfrak{D}$  modeling non-unitary dynamics on the system, such as quantum decoherence and energy relaxation. The dissipator is given in terms of the Lindblad operators  $\{\hat{L}_j\}$  and  $\hat{\rho}$ :

$$\mathfrak{D} \equiv \sum_{j=1}^s \hat{L}_j \hat{\rho} \hat{L}_j^\dagger - \frac{1}{2} \left\{ \hat{L}_j^\dagger \hat{L}_j, \hat{\rho} \right\} . \quad (\text{A.16})$$

The next step is to differentiate the energy equation of (A.14) to obtain an expression for  $p$ , the rate of work done on the system:

$$p \equiv \dot{E} = \frac{d}{dt} \text{Tr} \left( \hat{H} \hat{\rho} \right) = \text{Tr} \left( \frac{d}{dt} \left( \hat{H} \hat{\rho} \right) \right) , \quad (\text{A.17})$$

Here, the linearity of the trace and the derivative allow us to swap the order of operations. Since  $E$  is system energy,  $p$  and its components are to be considered as power input to the system ( $p > 0$  raises  $E$ , and  $p < 0$  lowers  $E$ ).

By the product rule, the power equation becomes

$$p = \text{Tr} \left( \dot{\hat{H}}\hat{\rho} + \hat{H}\dot{\hat{\rho}} \right) = \overbrace{\text{Tr} \left( \dot{\hat{H}}\hat{\rho} \right)}^{\text{A}} + \overbrace{\text{Tr} \left( \hat{H}\dot{\hat{\rho}} \right)}^{\text{B}}, \quad (\text{A.18})$$

where the linearity of the trace has been used to make the trace of a sum into a sum of traces, which we label A and B. The Lindblad operators  $\{\hat{L}_j\}$  act only on the Hilbert space of the vibronic system. The Hamiltonian is given by

$$\hat{H} = \hat{H}_e + \hat{H}_{ev} + \hat{H}_v, \quad (\text{A.19})$$

where  $\hat{H}_e$  and  $\hat{H}_v$  are the free Hamiltonian operators for the electron and the odorant vibrational modes, respectively; and  $\hat{H}_{ev}$  describes the electron-vibration coupling. An assumption valid in this context is that  $\dot{\hat{H}} = 0$ . Thus, only term B of (A.18) is nonzero and the rate of work done on the system is:

$$\begin{aligned} p &= \text{Tr} \left( \hat{H}\dot{\hat{\rho}} \right) \\ &= \text{Tr} \left( \hat{H} \left( -\frac{i}{\hbar} [\hat{H}, \hat{\rho}] + \mathfrak{D} \right) \right) \\ &= -\frac{i}{\hbar} \text{Tr} \left( [\hat{H}, \hat{\rho}] \hat{H} \right) + \text{Tr} \left( \mathfrak{D} \hat{H} \right). \end{aligned} \quad (\text{A.20})$$

Next, the Hamiltonian may be expanded as in (A.19) so that we can write (A.20) as

$$\begin{aligned} p &= \sum_{\alpha,\beta} -\frac{i}{\hbar} \text{Tr} \left( [\hat{H}_\alpha, \hat{\rho}] \hat{H}_\beta \right) + \sum_{\gamma} \text{Tr} \left( \mathfrak{D} \hat{H}_\gamma \right) \\ &= \sum_{\alpha,\beta} p_{\alpha,\beta} + \sum_{\gamma} p_{\mathcal{E},\gamma}, \end{aligned} \quad (\text{A.21})$$

where

$$p_{\alpha,\beta} = -\frac{i}{\hbar} \text{Tr} \left( [\hat{H}_\alpha, \hat{\rho}] \hat{H}_\beta \right), \quad \alpha, \beta \in \{e, ev, v\} \quad (\text{A.22})$$

is the power flow between the electronic, electron-vibron coupling, and vibronic, sub-components; and,

$$p_{\mathcal{E},\gamma} = \text{Tr} \left( \mathfrak{D} \hat{H}_\gamma \right) , \quad \gamma \in \{e, ev, v\} \quad (\text{A.23})$$

is the power input from the environment to the electronic, electron-vibron coupling, and vibronic, subcomponents of the open system.

The first sum in (A.21) reduces to zero since three of the  $p_{\alpha,\beta} = 0$  when  $\alpha = \beta$ , and the remaining six cancel because they are pairs of opposites  $p_{\alpha,\beta}$  and  $p_{\beta,\alpha}$  ( $\alpha \neq \beta$ ). Thus, component B of (A.18) reduces to

$$p = \sum_{\gamma} p_{\mathcal{E},\gamma} . \quad (\text{A.24})$$

There is only one source power into the electron+vibron system: the environment, which does work on the components of system at rate  $p_{\mathcal{E},ev} + p_{\mathcal{E},v} + p_{\mathcal{E},e}$ .

Finally, we identify, power dissipation  $p_{\text{diss}}$  from the electron-vibron system to the environment as:

$$p_{\text{diss}} = -p_{\mathcal{E},ev} - p_{\mathcal{E},v} - p_{\mathcal{E},e} . \quad (\text{A.25})$$

## REFERENCES

- [1] Antranik.org. Chemical sense: Smell (olfaction). [Online]. Available: <https://antranik.org/chemical-sense-smell-olfaction/>
- [2] J. Brookes, F. Hartoutsiou, A. Horsfield, and A. Stoneham, “Could humans recognize odor by phonon assisted tunneling?” *Phys Rev Lett*, vol. 98, p. 038101, January 2007.
- [3] I. Khemis, N. Mechi, and A. Lamine, “Stereochemical study of mouse muscone receptor mor215-1 and vibrational theory based on statistical physics formalism,” *Prog. Biophys. Mol. Bio.*, vol. 136, pp. 54–60, 2018.
- [4] A. Keller and L. Vosshall, “A psychophysical test of the vibration theory of olfaction,” *Nature Neurosci.*, vol. 7, no. 4, pp. 337–338, April 2004.
- [5] M. Franco, L. Turin, A. Mershin, and E. Skoulakis, “Molecular vibration-sensing component in drosophila melanogaster olfaction,” *P. Natl. Acad. Sci. USA*, vol. 108, no. 9, pp. 3797–3802, March 2011.
- [6] S. Gane, D. Georganakis, K. Maniati, M. Vamvakias, N. Ragoussis, E. Skoulakis, and L. Turin, “Molecular vibration-sensing component in human olfaction,” *PLoS One*, vol. 8, no. 1, p. e55780, 2013.
- [7] E. Block, S. Jang, H. Matsunami, S. Sekharan, B. Dethier, M. Ertem, S. Gundala, Y. Pan, S. Li, Z. Li, S. Lodge, M. Ozbil, H. Jiang, S. Penalba, V. Batista, and H. Zhuang, “Implausibility of the vibrational theory of olfaction,” *P Natl Acad Sci USA*, vol. 112, no. 21, pp. E2766–E2774, 2015.
- [8] L. Turin, S. Gane, D. Georganakis, K. Maniati, and E. Skoulakis, “Plausibility of the vibrational theory of olfaction,” *P Natl Acad Sci USA*, vol. 112, no. 25, p. E3154, 2015.
- [9] E. Block, S. Jang, H. Matsunami, V. S. Batista, and H. Zhuang, “Reply to turin et al.: vibrational theory of olfaction is implausible,” *Proc. Natl. Acad. Sci. US*, vol. 112, no. 25, pp. E3155–E3155., 2015.
- [10] M. Paoli, A. Anesi, R. Antolini, G. Guella, G. Vallortigara, and A. Haase, “Differential odour coupling of isoptomers in the honeybee brain,” *SCI REP-UK*, vol. 6, p. 21893, 2016.

- [11] E. Drimyli, A. Gaitanidis, K. Maniati, L. Turin, and E. M. Skoulakis, “Differential electrophysiological responses to odorant isotopologues in drosophilid antennae,” *eNeuro*, pp. ENEURO–0152, 2016.
- [12] J. Brookes, A. Horsfield, and A. Stoneham, “The swipe card model of odorant recognition,” *Sensors*, vol. 12, pp. 15 709–15 749, 2012.
- [13] L. Turin, “A spectroscopic mechanism for primary olfactory reception,” *Chem Senses*, vol. 21, pp. 773–791, 1996.
- [14] R. Hoehn, D. Nichols, H. . Neven, and S. Kais, “Status of the vibrational theory of olfaction,” *Frontiers Phys*, vol. 6, p. 25, 2018.
- [15] I. Solv’yov, P.-Y. Chang, and K. Schulten, “Vibrationally assisted electron transfer mechanism of olfaction: myth or reality?” *Phys. Chem. Chem. Phys.*, vol. 14, pp. 13 861–13 871, 2012.
- [16] E. Bittner, A. Madalan, A. Czader, and G. Roman, “Quantum origins of molecular recognition and olfaction in drosophila,” *J. Chem. Phys.*, vol. 137, p. 22A551, 2012.
- [17] A. Checinska, F. Pollock, L. Heaney, and A. Nazir, “Dissipation enhanced vibrational sensing in an olfactory molecular switch,” *J. Chem. Phys.*, vol. 142, p. 025102, 2015.
- [18] A. Tirandaz, F.T. Ghahramani, and V. Salari, “Validity examination of the dissipative quantum model of olfaction,” *SCI REP-UK*, vol. 7, p. 4432, 2017.
- [19] J. Brookes, “Quantum effects in biology: golden rule in enzymes, olfaction, photosynthesis and magnetodetection,” *Proc. R. Soc. A*, vol. 473, no. 20160822, 2017.
- [20] A. Tirandaz, F. Ghahramani, and A. Shafiee, “Dissipative vibrational model for chiral recognition in olfaction,” *Phys. Rev. E.*, vol. 92, p. 032724, 2015.
- [21] H. Breer, “Olfactory receptors: Molecular basis for recognition and discrimination of odors,” *Analytical and bioanalytical chemistry*, vol. 377, pp. 427–33, 11 2003.
- [22] L. B. Buck and R. Axel, “A novel multigene family may encode odorant receptors: A molecular basis for odor recognition,” *Cell*, vol. 65, pp. 175–187, 1991.
- [23] L. Haffenden, V. Yaylayan, and J. Fortin, “Investigation of vibrational theory of olfaction with variously labelled benzaldehydes,” *Food Chemistry*, vol. 73, pp. 67–72, 04 2001.
- [24] G. Dyson, “The scientific basis of odour,” *J. Soc. Chem. Ind.-L*, vol. 57, no. 28, pp. 645–664, July 1938.

- [25] G. Lindblad, “On the generators of quantum dynamical semigroups,” *Commun. Math. Phys.*, vol. 48, pp. 119–130, 1967.
- [26] J.-P. Vilaradaga, M. Bünemann, C. Krasel, M. Castro, and M. Lohse, “Measurement of the millisecond activation switch of g protein–coupled receptors in living cells,” *Nature Biotechnol.*, vol. 21, pp. 807–812, June 2003.
- [27] R. Hoehn, D. Nichols, H. Neven, and S. Kais, “Neuroreceptor activation by vibration-assisted tunneling,” *Sci Rep.*, vol. 5, p. 9990, 2014.
- [28] A. Patil, D. Saha, and S. Ganguly, “A quantum biomimetic electronic nose sensor,” *Scientific Reports*, vol. 8, 12 2018.
- [29] C. M. Willis, S. M. Church, C. M. Guest, W. A. Cook, N. McCarthy, A. J. Bransbury, M. R. T. Church, and J. C. T. Church, “Olfactory detection of human bladder cancer by dogs: proof of principle study,” *BMJ*, vol. 329, no. 7468, pp. 712–712, Sep 2004. [Online]. Available: <https://www.ncbi.nlm.nih.gov/pubmed/15388612>